GEODYNAMICS & TECTONOPHYSICS

PUBLISHED BY THE INSTITUTE OF THE EARTH'S CRUST
SIBERIAN BRANCH OF RUSSIAN ACADEMY OF SCIENCES

2015 VOLUME 6 ISSUE 2 PAGES 133–170 ISSN 2078-502X

http://dx.doi.org/10.5800/GT-2015-6-2-0176

COMPLEX GEOLOGICAL–GEOPHYSICAL 3D MODEL OF THE CRUST IN THE SOUTHEASTERN FENNOSCANDIAN SHIELD: NATURE OF DENSITY LAYERING OF THE CRUST AND THE CRUST–MANTLE BOUNDARY

V. N. Glaznev[1], M. V. Mints[2], O. M. Muravina[1], A. B. Raevsky[3], L. G. Osipenko[3]

[1] *Voronezh State University, Voronezh, Russia*
[2] *Geological Institute of RAS, Moscow, Russia*
[3] *Geological Institute, Kola Science Center of RAS, Apatity, Russia*

Abstract: The complex geophysical 3D model of the Earth's crust and the upper mantle is created for the Archaean Karelian Craton and the Late Palaeoproterozoic accretionary Svecofennian Orogen of the southeastern Fennoscandian Shield with the use of methods of complex inversion of geophysical data based on stochastic description of interrelations of physical properties of the medium (density, P-wave velocity, and heat generation). To develop the model, we use results of deep seismic studies, gravity and surficial heat flow data on the studied region. Numerical solutions of 3D problems are obtained in the spherical setting with an allowance for the Earth's surface topography. The geophysical model is correlated with the regional geological data on the surface and results of seismic CMP studies along 4B, FIRE-1 and FIRE-3-3A profiles. Based on results of complex geophysical simulation and geological interpretation of the 3D model, the following conclusions are drawn. (1) The nearly horizontal density layering of the continental crust is superimposed on the previously formed geological structure; rock differentiation by density is decreasing with depth; the density layering is controlled by the recent and near-recent state of the crust, but can be disturbed by the latest deformations. (2) Temperature variations at the Moho are partially determined by local variations of heat generation in the mantle, which, in turn, are related to local features of its origin and transformation. (3) The concept of the lower continental crust being a reflectivity zone and the concept of the lower continental crust being a layer of high density and velocity are not equivalent: the lower crust is the deepest, high-density element of near-horizontal layering, whereas the seismic image of the reflectivity zone is primarily related to transformation of the crust as a result of magmatic under- and intraplating under conditions of extension and mantle-plume activity. (4) At certain combinations of crustal thickness and temperature at the level of Moho discontinuity, the crust in a platform region can be transformed into eclogites. In this case, the crust–mantle boundary is determined by quantitative proportions of the rocks that underwent eclogitization or escaped this process and by corresponding density and velocity values. (5) High compaction of rocks in the crust under lithostatic loading cannot be explained by «simple» concepts of metamorphism and/or rock compaction, which are based on laboratory studies of rock samples and mathematical simulations; this is an evidence of the existence of additional, quite strong mechanisms providing for reversible changes of the rocks.

Key words: geophysical simulation, complex inversion, thermal model, density model, CMP seismic profiling, crustal–mantle boundary, velocity–density Moho discontinuity, Karelian Craton, Svecofennian Orogen.

Recommended by E.V. Sklyarov

For citation: *Glaznev V.N., Mints M.V., Muravina O.M., Raevsky A.B., Osipenko L.G.* 2015. Complex geological–geophysical 3D model of the crust in the southeastern Fennoscandian Shield: Nature of density layering of the crust and the crust–mantle boundary. *Geodynamics & Tectonophysics* 6 (2), 133–170. doi:10.5800/GT-2015-6-2-0176.

Комплексная 3-мерная геолого-геофизическая модель коры на юго-востоке Фенноскандинавского щита: природа плотностной расслоенности коры и коромантийной границы

В. Н. Глазнев[1], М. В. Минц[2], О. М. Муравина[1], А. Б. Раевский[3], Л. Г. Осипенко[3]

[1] *Воронежский государственный университет, Воронеж, Россия*
[2] *Геологический институт РАН, Москва, Россия*
[3] *Геологический институт КНЦ РАН, Апатиты, Россия*

Аннотация: Трехмерная комплексная геофизическая модель земной коры и верхней части мантии архейского Карельского кратона и позднепалеопротерозойского Свекофеннского аккреционного орогена на юго-востоке Фенноскандинавского щита получена с использованием методов комплексной инверсии геофизических данных, основанных на стохастическом описании взаимосвязей физических свойств среды: плотности, скорости продольных волн и теплогенерации пород. Для построения модели использованы результаты глубинных сейсмических исследований, данные о гравитационном поле и поверхностном тепловом потоке изучаемого региона. Численные схемы решения трехмерных задач реализованы в сферической постановке с учетом реального рельефа Земли. Методика достаточно универсальна и перспективна при исследовании строения коры и литосферы крупных регионов. Геофизическая модель сопоставлена с региональными поверхностными геологическими данными и результатами сейсмических исследований МОГТ по профилям 4В, FIRE-1 и FIRE-3-3A. По результатам комплексного геофизического моделирования и геологической интерпретации особенностей полученной объемной модели показано: (1) субгоризонтальная плотностная расслоенность континентальной коры накладывается на ранее сформированную геологическую структуру, плотностная дифференциация пород с глубиной уменьшается; особенности плотностной расслоенности в преобладающей степени определяются современным и относительно недавним состоянием коры, но могут быть нарушены в результате наиболее поздних деформаций; (2) температурные вариации на разделе Мохо частично определяются «локальными» изменениями теплогенерации мантии, которые обусловлены особенностями ее формирования и преобразования; (3) представления о нижней коре континентов как о «зоне рефлективити» и как о слое значительно повышенной плотности и скорости не являются эквивалентными: нижняя кора – это наиболее глубинный и наиболее высокоплотный элемент субгоризонтальной плотностной расслоенности, в свою очередь, сейсмический образ «зоны рефлективити» преимущественно связан с процессами преобразования коры в результате магматического андерплейтинга и интерплейтинга в обстановках рифтогенного растяжения и мантийно-плюмовой активности; (4) при определенных сочетаниях мощности коры и температурного режима на уровне раздела Мохо породы коры платформенных областей могут быть преобразованы в эклогиты – в этом случае граница коры и мантии определяется количественными соотношениями пород, подвергшихся и не подвергшихся эклогитизации, и соответствующими значениями плотностных и скоростных характеристик; (5) высокий уровень уплотнения пород в коре под воздействием литостатической нагрузки невозможно объяснить на уровне «простых» представлений о метаморфизме и/или об уплотнении и компакции пород, базирующихся на лабораторных исследованиях образцов и расчетных моделях, что свидетельствует о существовании дополнительных и весьма мощных механизмов, которые обеспечивают обратимые изменения горных пород.

Ключевые слова: геофизическое моделирование, комплексная инверсия, термическая модель, плотностная модель, сейсмопрофилирование МОГТ, граница кора-мантия, сейсмоплотностной раздел Мохо, Карельский кратон, Свекофеннский ороген.

Contents

1. INTRODUCTION

In studies of deep structure of the crust and upper mantle, the most appropriate approach is using a complex of geophysical methods [*Glaznev, 2003*]. Meanwhile, some properties of the geological medium, which are determined by different geophysical methods cannot be successfully combined under the common framework of complex models. It is thus required to examine two or more independent models. In particular, it is well known that images of the crust – mantle boundary and structural–compositional layering established by refraction seismic methods (including the models, where velocity characteristics of the medium are interpreted in combination with gravity data) differ in principle from those based on reflection seismic methods.

Although the Moho discontinuity has been known for more than a century, determining the origin and formation conditions of the Moho, as well as crust–mantle boundary remains one of the main problems in studying the lithosphere [*Carbonell et al., 2013; Prodehl et al., 2013*]. Historically, many authors consider terms *crust–mantle boundary* and *Moho discontinuity* as synonyms. With enhancement of our knowledge on the transitional zone and the crust–mantle boundary proper, it has become evident that these notions do not coincide completely. The Moho is a geophysical image of the smoothly curving surface of the planetary rank, at intersection of which P-wave velocity increases more or less abruptly from 6.9–7.4 to 8.0–8.2 km/s. This surface is approximately following the lower boundary of the Earth's crust. The crust–mantle boundary is a complex geological phenomenon characterized by a combination of data on composition, metamorphic grade, and mechanical properties of the crust, mantle and transitional zone, as well as on structural features of the crust–mantle boundary. Further in the text, we use term *Moho boundary or discontinuity* for notation of the velocity boundary in the transitional crust–mantle zone. In discussion of structural and compositional features of the boundary and/or the transitional zone between the crust and the mantle, we use geological terms *crust–mantle boundary / interface.* In general, the Moho discontinuity and the crust–mantle boundary may be not coincident [*O'Reilly, Griffin, 2013*].

The geological structure of the crust–mantle boundary can be characterized, in particular, by patterns of seismic reflections (seismic images). The Moho discontinuity may be situated both above and below this boundary. In some cases, the crust–mantle boundary remains unchanged from the time of crust formation, whereas in other cases, it is younger than the major part of the overlying crust [*Braile, Chiangl, 1986; Mereu et al., 1989; Mooney, Meissner, 1992; Berzin et al., 2002; Cook et al., 2010; Mints, 2011*].

Reflection seismic methods yield widely variable seismic images of the crust–mantle boundary at the base of Precambrian crust, and specific features of such images suggest a dependence on structure and formation history of the crust [*BABEL Working Group, 1990; Abramovitz et al., 1997; White et al., 2000; Van der Velden, Cook, 2005; Kukkonen, Lahtinen, 2006; Mints et al., 2009, 2015; Cook et al., 2010; Hammer et al., 2010; Mints, 2011*]. It is assumed that beneath the Precambrian cratons, as a rule, this boundary is rather distinctly expressed in the replacement of the moderately or intensely reflecting lower crust by the mantle domain that is acoustically transparent. To determine a true vertical depth of the crust–mantle boundary, the crustal velocity structure should be known. If the CMP profiles are not accompanied by refraction seismic studies, uncertainty in determination of depth can reach 5–6 % [*Holbrook et al., 1992*].

The studies of P-wave velocities with application of refraction seismic methods have shown that the Earth's crust is subdivided in several «layers» that differ in velocities of acoustic signal propagation and are separated by distinct and, in other cases, vague boundaries or diffuse gradient zones. Statistically persistent corre-

lations between density and velocity parameters of rocks make it possible to jointly discuss velocity layering and density layering of the crust [*Christensen, Mooney, 1995*]. As a rule, velocity (V_p) and density (ρ) progressively increase with depth.

Velocity and density layering of the crust in the central Fennoscandian Shield was described in [*Korsman et al., 1999; Kozlovskaya et al., 2004; Kuusisto et al., 2006; Silvennoinen et al., 2014*]. In particular, these authors established gradual variations of velocity and density within the crustal «layers», which number may amount to six according to [*Kuusisto et al., 2006*].

In this paper, we focus on the key region located at the junction of two tectonic units differing in structure and age, the Archaean Karelian Craton and the Late Palaeoproterozoic accretionary Svecofennian Orogen. Our study is aimed at establishing structural and compositional layering of the crust, nature of crust–mantle boundary, and the present-day thermodynamic state of the boundary zone between the crust and the upper mantle.

A fragment of the 3D complex geophysical model of the Fennoscandian crust and upper mantle is used as the major tool. It characterizes relationships between P-wave velocity, density, heat generation, and thermal conductivity of rocks, which determine gravity field, surficial heat flow, and internal fields of temperature and lithostatic pressure [*Glaznev et al., 1996; Glaznev, 2003*]. Seismic images of the crust along detailed 4B, FIRE-1, FIRE-3-3A CMP profiles and corresponding geological interpretation sections [*Kukkonen, Lahtinen, 2006; Mints et al., 2009, 2015; Mints, 2011*] are used as the second independent model.

The efficient modern methods for 3D geophysical (petrophysical) modeling of the Earth's crust are based on the criteria–target–oriented approach [*Strakhov, Romanyuk, 1984; Golizdra, 1988*], which assumes a combination of the solutions obtained using a complex of geophysical methods within a certain coherent presentation of interpretational petrophysical parameters characterizing the geological medium [*Glaznev, 1987, 2003; Glaznev et al., 1989, 1996, 2008; Buyanov et al., 1995; Romanyuk, 1995; Romanyuk et al., 2001; Tiberi et al., 2003; Kozlovskaya et al., 2004; Artemieva et al., 2006; Kobrunov, 2008; Tikhotsky, Achauer, 2008*]. Nevertheless, issues of adequacy of the mathematical tool used for compilation of coordinated complex geophysical models of the medium in various situations has not been scrutinized yet to a sufficiently detailed level. This especially concerns identification of non-horizontal layering of the Earth's crust, which is only partly reflected in the available models. It is also evident that the criteria–target–oriented approach leads to a certain generalization of the studied medium structure that depends on discreteness of the network representation of relevant physical properties.

2. Principles and methods of complex interpretation

The technique of complex geophysical simulation of the crust was considered in detail in [*Glaznev et al., 1996; Glaznev, 2003*]. This paper is confined only to the description of the main principles and justification of this technique.

Let us consider statement of certain principal elements of the technique aimed at complex geophysical inversion of gravimetric and geothermal data on the basis of seismic data on structure of the crust and stochastic descriptions of interrelations between physical properties of rocks in the studied medium. The proposed algorithms to solve 3D complex inverse problem are considered in a spherical setting, taking into account a real surface of the Earth, because of significant dimensions (i.e. area and depth) of the simulated region. As a result of complex inverse problem solution, 3D thermal and density models are proposed for the crust and the upper mantle of the Karelian Craton and the adjacent territories of Fennoscandia. These models reflect the main features of the deep structure of the studied region.

The crustal rocks are characterized by velocity of P-waves V, density ρ, heat generation q, and heat conductivity λ, which generate the external observable gravity field $\Delta g(x)$ and the field of surficial heat flow $Q(x)$ as well as the internal fields of temperature T(ξ) and lithostatic pressure $P(\xi)$ in the medium. It is assumed that the sought physical properties of the medium (V, ρ, q) are characterized by stochastic interrelations, which can be described by certain sets of statistic parameters.

Taking into account the availability of a priory velocity model, the problem of complex interpretation is defined as a calculation of 3D thermal and density models on the basis of inverse problem solutions of geothermal and gravimetric data. Following the principle described in [*Strakhov, Romanyuk, 1984; Glaznev, 1987*] for selection of solutions that can ensure (within the given confidence interval) the correspondence of solutions to the accepted law of relationships between parameters, the procedure of complex interpretation is stated as follows:

$$\left\| A_{\Delta g}\{p(\xi), p_N(\xi)\} - \Delta g(x) \right\| = \delta_{\Delta g}, \qquad (1)$$

$$\left\| A_Q\{q(\xi),\ \lambda(\xi)\} - Q(x) \right\| = \delta_Q, \tag{2}$$

where $A_{\Delta g}\{\}$ and $A_Q\{\}$ are operators of the corresponding direct problems; $\rho(\xi)$ and $q(\xi)$ are the sought density and heat generation values; $\rho_N(\zeta)$ is the one-dimensional normal density in medium; $\lambda(\xi)$, thermal conductivity of medium; $\Delta g(x)$ and $Q(x)$ are observed gravity field and field of surficial heat flow; ξ and x are integrated coordinates of field sources and observation points; $\delta_{\Delta g}$ and δ_Q are discrepancies of fields. Solution quality functionals based on stochastic descriptions of the relationship between density, heat generation, and velocity in medium [*Glaznev, 2003*] are defined as follows:

$$\int_v W_\rho(\xi) \cdot \left(\rho(\xi) - \rho_{\text{ini}}(\xi)\right)^2 dv = \min, \tag{3}$$

$$\int_v W_q(\xi) \cdot \left(q(\xi) - q_{\text{ini}}(\xi)\right)^2 dv = \min, \tag{4}$$

where $W_\rho(\xi)$ and $W_q(\xi)$ are weight functions for density and heat generation models of medium expressed via entropic characteristics of density–velocity and heat generation–density distributions; $\rho_{\text{ini}}(\xi)$ and $q_{\text{ini}}(\xi)$ are initial approximations of density and heat generation models based on initial velocity model of the medium. According to [*Strakhov, 1990*], smallness of solution fluctuation versus initial approximation, as well as limitation of $W_\rho(\xi)$ and $W_q(\xi)$ weight function are assumed.

Initial approximations $\rho_{\text{ini}}(\xi)$ and $q_{\text{ini}}(\xi)$ for models of the medium can be expressed through velocity $V(\xi)$ based on approximation density–velocity $\rho=f_\rho(V)$ and heat generation–density $q=f_q(\rho)$ relationships. The dependence of these physical properties on thermodynamic conditions in the medium should be taken into account:

$$\rho_{ini}(\xi) = f_\rho\left(V(\xi) - \int (dV/dP)_T\, dP - \int (dV/dT)_P\, dT\right) + \int (d\rho/dP)_T\, dP + \int (d\rho/dT)_P\, dT, \tag{5}$$

$$q_{ini}(\xi) = f_q\left(\rho(\xi) - \int (d\rho/dP)_T\, dP - \int (d\rho/dT)_P\, dT\right), \tag{6}$$

where $(dV/dP)_T$ and $(dV/DT)_P$ are isothermal and isobaric corrections to velocity; $(d\rho/dP)_T$ and $(d\rho/dT)_P$ are similar corrections to density established from results of integration of experimental data on rock samples from the lithosphere [*Glaznev et al., 1996; Glaznev, 2003*].

The critical aspect in the problem of complex inversion is the use of limitations on values of sought solutions:

$$\rho_{j\,min} \le \rho(\xi_j) \le \rho_{j\,max}, \tag{7}$$

$$q_{j\,min} \le q(\xi_j) \le q_{j\,max}, \tag{8}$$

where $j \in [1, M]$ are corresponding minimum and maximum values set for certain finite subregions of medium j. Such limitations need to be taken due to geological reasoning and on the basis of a priori classification requirements [*Buyanov et al., 1989*]. In addition, solution of inverse problems takes into account the data obtained from petrophysical (density) regional mapping [*Galitchanina et al., 1995*] and estimations of heat generation of the rocks occurring at the surface, which are a priori boundary values for density $\rho_S(\xi)$ and heat generation $q_S(\xi)$ of the rocks occurring at the surface $h(x)$ of the studied medium:

$$\rho(\xi)|_{\xi=h(x)} = \rho_S(h), \tag{9}$$

$$q(\xi)|_{\xi=h(x)} = q_S(h). \tag{10}$$

The computation algorithm of complex interpretation in the setting (Eqs. 1–10) is determined by the initial velocity model of the medium, which is considered to be the constant basis. This model corresponds to a certain initial distribution of density $\rho^{(0)}(\xi)$ and heat generation $q^{(0)}(\xi)$ in the studied medium. At the first step of complex interpretation, the 3D thermal model $T^{(1)}(\xi)$ is computed and heat generation $q^{(1)}(\xi)$ is specified from

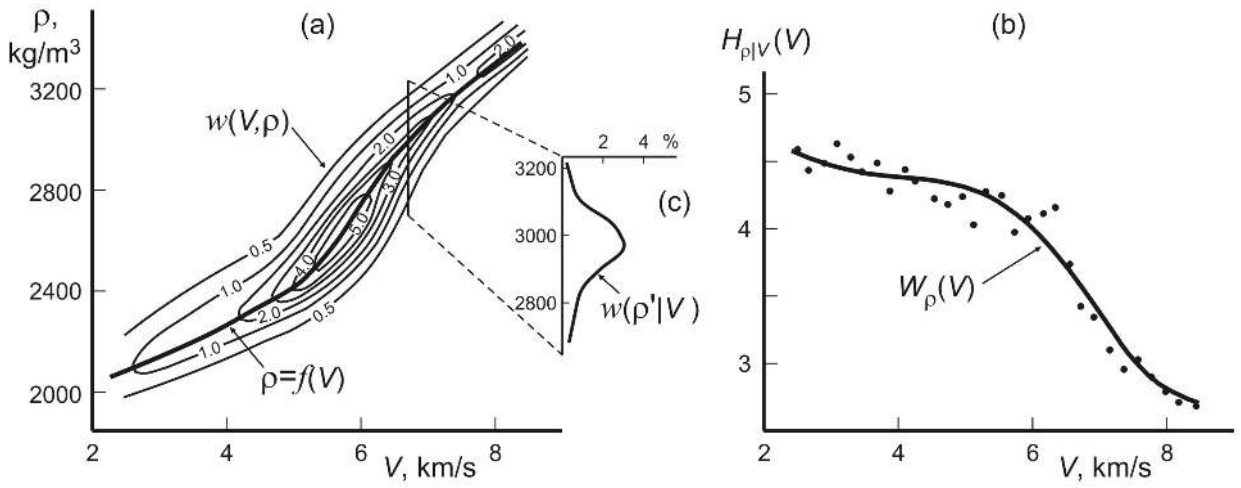

Fig. 1. (*a*) Stochastic interrelations between P-wave velocity (V) and density (ρ) of crustal rocks in form of 2D probability distribution (contour lines, %) and approximation graph ρ=$f(V)$ (Eq. 11). (*b*) Conditional probability density $w(ρ|V)$ in a section of 2D process $w=w(V,ρ)$. (*c*) Calculated entropy $H_{ρ|V}(V)$ and approximation of weight function $W_ρ(V)$ (Eq. 13).

Рис. 1. (*a*) Стохастическая взаимосвязь между скоростью и плотностью пород земной коры в виде двухмерного распределения вероятности (изолинии в процентах) и график аппроксимации ρ=$f(V)$ в форме (11). (*b*) Условная плотность вероятности $w(ρ|V)$ по некоторому сечению двумерного процесса $w=w(V,ρ)$. (*c*) Вычисленные значения энтропии $H_{ρ|V}(V)$ и аппроксимация весовой функции $W_ρ(V)$ в форме (13).

the solution of the inverse geothermal problem (Eqs. 2, 4, 6, 8, 10). At the second step, medium density $\rho^{(1)}(\xi)$ is computed and lithostatic pressure $P^{(1)}(\xi)$ is specified from the solution of the inverse gravimetric problem (Eqs. 1, 3, 5, 7, 9). The obtained coordinated model of temperature, heat generation, and density is further specified at the next steps of iteration cycle to ensure more accurate correspondence of models to one another on the basis of a priori accepted stochastic interrelations of the physical properties.

The important aspect of this simulation is establishing interrelations between P-wave velocity, density, and heat generation. The stochastic interrelations between velocity and density under normal thermodynamic conditions have been revealed for typical lithospheric rocks [*Glaznev et al., 1996; Glaznev, 2003*]. As a function of mutual density–velocity transition, the following approximation is proposed:

$$\rho = f(V) = a + b \cdot ln(|V + c|), \tag{11}$$

where a, b, and c coefficients determined for two velocity ranges: (1) a=2933, b=–518, and c=–7.985 at $V \leq 5.5$ km/s; (2) a=1656, b=1068, and c=–3.181 at V>5.5 km/s. Dimensions of velocity and density in Eq. 11 are given in km/s and kg/m^3, respectively. Graphs of $\rho = f(V)$ in corresponding velocity ranges are shown in Fig. 1, *a*. It is noteworthy that Eq. 11 coincides with known density–velocity relationships [*Birch, 1961; Ludwig et al., 1970; Barton, 1986; Sobolev, Babeyko, 1994*] for sedimentary and crystalline rocks and was efficiently used for development of geophysical models of the Earth's crust in various regions [*Vernant et al., 2002; Miksat et al., 2010*].

The stochastic character of transition from P-wave velocity to density can be expressed via entropy of conditional density probability of 2D accidental process $w(ρ|V)$ shown in Fig. 1, *b*. From definition of conditional entropy

$$H_{ρ|V}(V) = -\int_{-\infty}^{+\infty} w(\rho'|V) \cdot \log_2 w(\rho'|V) \cdot d\rho', \tag{12}$$

one can calculate a weight function that characterizes ambiguity of relationship between velocity and density. Approximation of calculated entropy values shown in Fig. 1, *c* is given by equation

$$W_\rho(V) = H_{ρ|V}(V) = \sum_{n=0}^{4} d_n \cdot (V)^n, \tag{13}$$

where constants d_0=10.365, d_1=–5.195, d_2=1.637, d_3=–0.2173, and d_4=–0.0099; velocity dimension is km/s. A graph of approximation $W_\rho(V)$ is shown in Fig. 1, *c*. The equations shown in Figs. 11 and 13 describe empirical statistical density vs. velocity under normal thermodynamic conditions and also characterize a measure of its uncertainty.

The relationships between density and heat generation for typical rocks in the lithosphere were introduced in the same way [*Glaznev, 2003*] and used for development of the thermal model of the region under consideration. In addition, an integrated relationship of thermal conductivity versus temperature figuring in Eq. 2 was introduced into the thermal model in form

$$\lambda(T) = \lambda_0(1 + c \cdot T)^{-1}, \tag{14}$$

where constant λ_0 and *c* for crystalline crustal rocks were chosen for two temperature intervals. In the range up to 900 K, λ_0=3.5 W/m·K and *c*=1.2·103 K^{-1}. In the range from 900 to 1200 K, λ_0=0.8 W/m·K and *c*=–5.8·10^{-4} K^{-1}. The relationship of thermal conductivity versus pressure was taken in linear approximation after [*Seipold, 1998*].

The methods of direct gravimetry problem solution are of substantial importance for procedure of complex simulation. In our case, they are realized in the 3D spherical setting [*Glaznev, Raevsky, 1991*] based on precise expressions for gravity field from a spherical disc in its polar point. The calculation of anomalous fields is based on the radial–ring overlay grid for a set of thin spherical rectangular sheets. For Δg field of thin spherical rectangle with constant $\Delta\rho$ density, we have

$$\Delta g(r,0,0) = \gamma\psi_m\Delta\rho\frac{R^2}{r^2}\left(\frac{R - r\cos\theta_{m+1}}{r_{m+1}} + \frac{R - r\cos\theta_m}{r_m}\right)dR, \tag{15}$$

where

$$r_m^2 = R^2 + r^2 - 2Rr\cos\theta_m, \qquad r_{m+1}^2 = R^2 + r^2 - 2Rr\cos\theta_{m+1},$$
$$r = R_0 + h, \qquad R = R_0 - z,$$

in which R_0 is the Earth's radius and *h* is the height of field calculation point. For the rectangle: $\psi_m = (\varphi_{n+1} = \varphi_n)$ in longitude and $(\theta_{m+1} - \theta_m)$ in latitude, optimal angular sizes are determined from conditions of field calculation accuracy and the requirement of approximate isometry of the spherical element of the network. The total gravitational effect from approximation of the medium by such elements is given as follows:

$$\Delta g(h,\phi,\theta) = \left(\sum_{k=0}^{K}\sum_{m=0}^{M}\sum_{n=0}^{N_m} C_{kmn}\cdot\Delta\rho(k,m,n) + \sum_{k=0}^{K} C'_k\cdot\Delta\bar{\rho}_M(k)\right)dR, \tag{16}$$

where variable indices *k, m,* and *n* operate in local polar coordinates, and C_{kmn} coefficients are calculated for a single element from the formula given above (C'_k are coefficients taking into account the effect of the far spherical zone).

The 3D inversion of gravimetric data is stated as a problem of finding such a distribution of density $\Delta\rho(r,\varphi,\theta)$, which satisfies a minimum of discrepancy (Eq. 1) for Δg field and minimizes solution quality functional (Eq. 3). The inverse problem in that setting was considered in various aspects by many authors [*Kobrunov, 1982, 2008; Dolgal, 2002; Pedersen, 1991; Tarantola, Valette, 1982*]. However, in our case, the weight functions $W(r,\varphi,\theta)$ for the density model of the medium are determined through entropic characteristics of velocity–density interrelations (Eq. 13).

For practical realization of the iteration algorithm of inversion, two stages are distinguished in the solution of inverse problem: calculation of the simple layer density, and its equivalent redistribution over the mass-carrier region. Calculation of the equivalent layer density can be regarded as a certain approximate solution of the inverse problem for the given set of discrete elements of the medium approximation [*Aleksidze, 1987*]. In the spherical setting, coefficients of the approximate inverse operator of determining the equivalent density of the simple spherical layer were obtained [*Glaznev, 2003*]. These coefficients are used in specific computational schemes.

The equivalent rearrangement from a thin layer (thickness Δh) into the model layer (thickness $N\Delta h$) is performed following the iteration scheme, and the following equation is obtained for density in layer *n*:

$$\Delta\rho^{(i+1)}(n,\varphi,\theta) = \Delta\rho^{(i)}(n,\varphi,\theta) + W_\rho(n)\cdot\left(\Delta\rho_e^{(i)}(\varphi,\theta)D(n,\varphi',\theta')\right), \tag{17}$$

where $\Delta\rho_e(\varphi,\theta)$ is the equivalent density for approximation $\Delta\rho(\varphi,\theta) - \Delta\rho^{(i)}(\varphi,\theta)$, and redistribution operator $D(n,\varphi,\theta)$ in spectral form assumes explicit presentation in form of binomial series of analytical continuations for the potential field. For the central point of the local polar spherical system of coordinates, with a limited number of members in this series, the second item in the right part of Eq. 17 is given as follows:

$$\Delta\rho(n,0,0) = \frac{1}{2}\sum_{m=0}^{M} C(n,m)_D \cdot \left(\Delta\bar{\rho}_e(R,\theta'_m) + \Delta\bar{\rho}_e(R,\theta'_{m+1})\right), \tag{18}$$

where equivalent density values are taken as average values at the circumferences. The cubature coefficients are

$$C_{(n,m)_D} = \sum_{p=0}^{3}(-1)^p R \int_{\theta'_m}^{\theta'_{m+1}} \frac{(R^2 - r^2(n,p)) \cdot \sin(p+1-n) \cdot \sin\theta'}{(R^2 + r^2(n,p) \cdot 2\mathrm{Rr}(n,p) \cdot \cos\theta')^{3/2}} d\theta' , \tag{19}$$

where $r(n,p)=R-(p+1-n)\Delta h$. The choice of a small number of members in series (Eqs. 18, 19) actually realizes the method of local redistribution of corrections [*Martushko, Prutkin, 2003*] in the problem of model layer density calculation.

The above-described technology of complex geophysical simulation was efficiently used for creation of the Earth's crust models under various conditions [*Buyanov et al., 1989, 1995; Glaznev et al., 1996, 2008*]. The same technology of inversion of 3D gravimetric and geothermal data in the spherical setting is applied for complex geophysical simulation of the Earth's crust in the Karelian Craton.

3. Geological overview

The studied area is situated in the southeastern Fennoscandian Shield in the territories of Russia and Finland (Fig. 2, *a*, *b*). The Karelian Craton and the Belomorian Province, that extends along the craton's eastern boundary, embrace the major in size and geological significance domains of the continental crust in the Fennoscandian Shield [*Mints et al., 2015*]. The crust was largely formed by the onset of the Neoarchaean and then underwent tectonic and metamorphic reworking during the Neoarchaean and Palaeoproterozoic. The volcanic–sedimentary and volcanic–plutonic associations of the Late Palaeoproterozoic Svecofennian Accretionary Orogen are bordering on the Karelian Craton in the southeast. The Archaean crustal granite–greenstone domains (GGD) making up the Late Palaeoproterozoic Karelian Craton are regarded as fragments of ancient microcontinents somewhat different in age. The Ranua, Iisalmi and Vodlozero GGDs are composed of the oldest granitoids dated at 3.14–2.82 Ga. The age of their protoliths reaches 3.5–3.7 Ga. The Kianta and Kuhmo–Segozero complexes mainly consist of tonalite–trondhjemite gneisses dated at 2.89–2.72 Ga.

The Archaean greenstone belts are subdivided into two groups. Mafic and ultramafic volcanic rocks play a significant role or are predominant in the first group. The extended linear belts of this group are considered as palaeosutures corresponding to collision events between the Segozero–Vedlozero, Central Belomorian, and Tipasjärvi–Kuhmo–Suomussalmi microcontinents (Fig. 2, *b*).

The Segozero–Vedlozero and Central Belomorian sutures arose 3.05–2.82 Ga ago. Rocks of the Tipasjärvi–Kuhmo–Suomussalmi suture are dated at 2.81–2.74 Ga. According to geological data and interpretation of seismic crustal images along CMP profiles 1-EU, 4B, FIRE-1 and FIRE-3-3A, all the three sutures plunge in the eastern and northeastern directions and are traced down to the crust–mantle boundary [*Mints et al., 2009, 2015*]. The younger belts of the second group, which are primarily composed of epicontinental metasedimentary and metavolcanic rocks, are dated at 2.75–2.73 Ga. These rocks are close in density to TTG and GG gneisses, do not reveal density anomalies, and thus are not shown in Fig. 2, *b*.

The Karelian Craton and Belomorian Province completed to evolve in the Neoarchaean (2.75–2.73 Ga ago). Later on, the crust was built up and reworked primarily in the intracontinental setting. The Varpaisjärvi and Chupa synforms composed of granulite-gneiss complexes appeared in the framework of the Karelian Craton 2.74–2.70 Ga ago as a result of mantle-plume activity. The granite–greenstone crust in the basement of these synforms was also affected by high-temperature granulite-facies metamorphism.

In the Early Palaeoproterozoic (~2.5–2.3 Ga ago), significant bodies of mafic igneous rocks, mainly of gabbroanorthosite composition, were accommodated at the base of the Archaean crust, which thickness

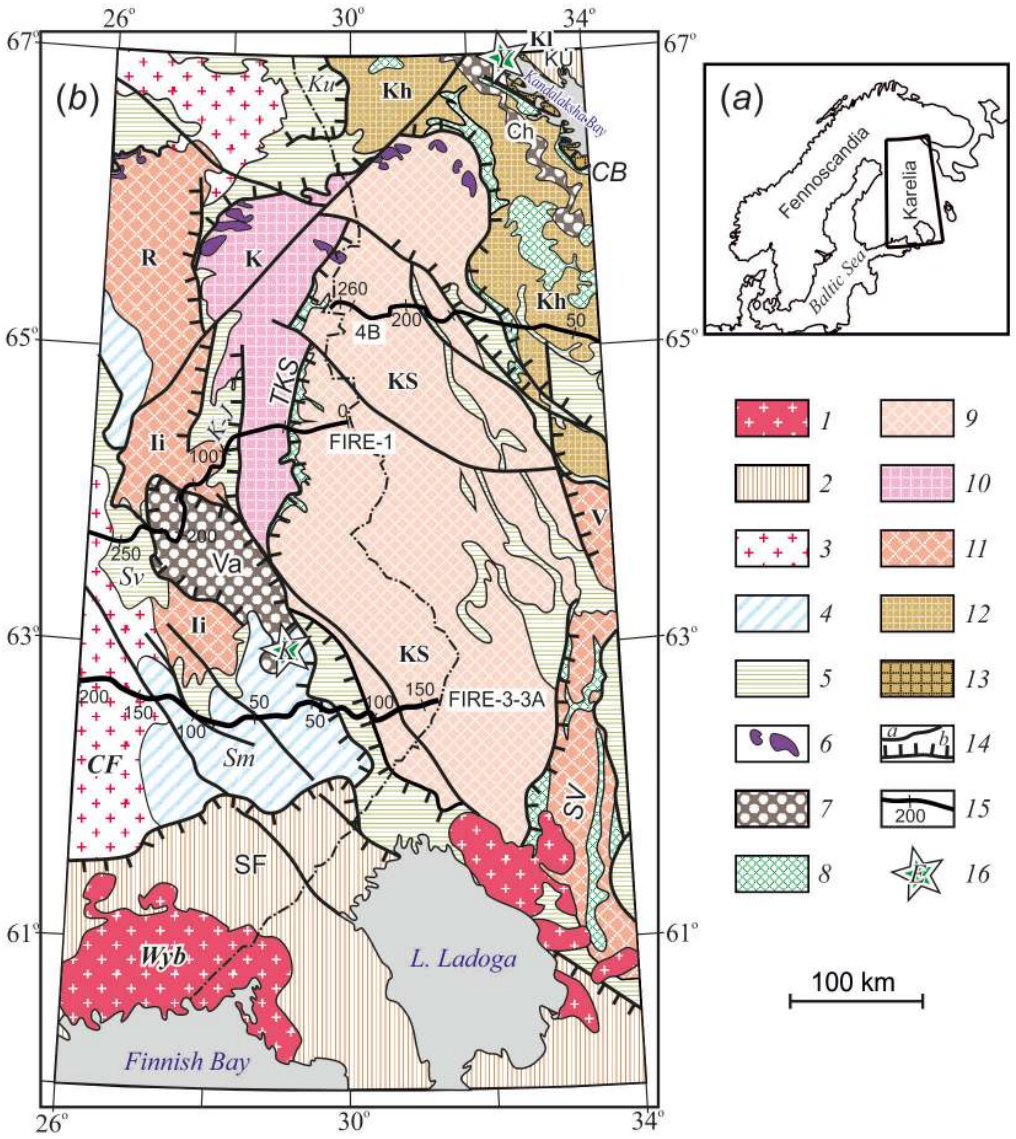

Fig. 2. (*a*) The geographical position of the area of effective integrated geophysical modeling. (*b*) Main tectonic units in the southeastern Fennoscandian Shield, simplified after [*Mints et al., 2015*].

1 – **Mesoproterozoic** rapakivi granites (Wyb, Wyborg pluton); *2–6* – **Palaeoproterozoic**: *2* – granulite-gneiss belts (SF – South Finland and KU – Kolvitsa–Umba); *3–4* – Svecofennian Orogen: *3* – granitoids (CF, Central Finland pluton), *4* – accretionary complex (Sv – Savo and Sm – Saimaa belts); *5* – volcanic–sedimentary belts (K-J – Kainuu volcanic–sedimentary belt containing Jormua ophiolite complex; Ku – Kuolajärvi structure); *6* – North Karelian belt, layered mafic–ultramafic intrusions; 7–12 – **Archaean**: *7* – granulite-gneiss belts (Va, Varpaisjärvi and Ch, Chupa), *8* – greenstone belts, inferred sutures (TKS, Tipasjärvi–Kuhmo–Suomussalmi, SV, Segozero–Vedlozero, and CB, Central Belomorian), *9–11* – Karelian Craton, granite–greenstone domains: *9* – Kuhmo–Segozero (KS), *10* – Kianta (Ki), *11* – Ranua (R), Iisalmi (Ii) and Vodlozero (V), *12* – Belomorian Province, Khetolambina granite–greenstone domain (Kh); *13* – Kola Craton (Kl); *14* – tectonic boundary: (*a*) normal–strike-slip fault, (*b*) thrust fault (ticks indicate direction of fault-plane plunging); *15* – 4B, FIRE-1 and FIRE-3-3A CMP seismic profiles; *16* – kimberlite pipes containing deep xenoliths (Y, Yelovy Island and K, Kaavi–Kuopio).

Рис. 2. (а) Географическое положение результативной области комплексного геофизического моделирования. (*b*) Главные тектонические структуры на юго-востоке Фенноскандинавского щита (упрощенно по [*Mints et al., 2015*]).

1 – **мезопротерозой**, граниты рапакиви (Wyb – Выборгский массив); *2–6* – **палеопротерозой**: *2* – гранулито-гнейсовые пояса (SF – Южно-Финляндский, KU – Колвица-Умбинский); *3–4* – Свекофеннский аккреционный ороген: *3* – гранитоиды (CF – Центрально-Финляндский плутон), *4* – аккреционный комплекс (пояса: Sv – Саво, Sm – Саимаа); *5* – осадочно-вулканогенные пояса (K-J – пояс Кайнуу, вмещающий офиолитовый комплекс Йормуа; Ku – Куолаярвинская структура); *6* – раннепалеопротерозойский Северо-Карельский пояс, расслоенные массивы мафит-ультрамафитов; *7–12* – **архей**: *7* – гранулито-гнейсовые пояса (Va – Варпаисърви, Ch – Чупинский), *8* – зеленокаменные пояса – предполагаемые палеосутуры (TKS – Типасъярви-Кухмо-Суомуссалми, SV – Сегозеро-Ведлозеро, CB – Центрально-Беломорскимй), *9–11* – **Карельский кратон**, террейны (гранит-зеленокаменные области): *9* – Кухмо-Сегозерский (KS), *10* – Кьянта (Ki), *11* – Рануа-Иисалми (R), Водлозерский (V), *12* – **Беломорская провинция**, Хетоламбинская гранит-зеленокаменная область (Kh); *13* – **Кольский кратон** (Kl); *14* – тектонические границы (а – сбросо-сдвиги, б – надвиги, штрихи указывают направление погружения сместителя); *15* – сейсмические профили МОГТ: 4B и FIRE-1; *16* – кимберлитовые трубки с глубинными ксенолитами (Y – Кандалакшский залив, остров Еловый, K – район Каави-Куопио).

reached 60–70 km at that time as a result of resumed mantle-plume activity. The intrusive bodies were subject to granulite-facies metamorphism along with the Archaean country rocks [*Mints et al., 2009, 2015*]. In the course of the Late Palaeoproterozoic tectonic compression, fragments of gabbroanorthosite bodies were transferred to the upper crust and accommodated at the base of tectono-stratigraphic sections of granulite-gneiss belts, mostly in the Lapland and Kolvitsa–Umba belts in the Kola Peninsula [*Mints et al., 1996*], whereas the predominant mass of gabroanorthosites remained at the level of the crust–mantle boundary. Almost synchronously with accommodation of gabbroanorthosites, mafic–ultramafic magmas were emplaced into the upper crust along the northern boundary of the Karelian Craton to form the North Karelian belt of layered intrusions. At the same time, the middle part of the crust in the Belomorian Province was intensely impregnated by small portions of mafic and ultramafic magma to form minor intrusions known as «drusites» (local name). At present, some of these intrusions are exposed at the surface.

The peak of rifting controlled by mantle-plume processes is most probably related to division of the large Archaean Lauroscandia continent (supercontinent) into the North American and East European parts and to opening of the Svecofennian paleoocean [*Mints, Konilov, 2004; Mints, 2007*]. In the same period of time, extended rifts filled with sediments, basalts and basaltic andesites were formed in the inner domain of the Karelian Craton. Rifting and related volcanic activity developed with breaks up to the end of the Palaeoproterozoic. The second peak of mantle-plume magmatism is dated at the Late Palaeoproterozoic, 2.2–1.8 Ga. The stage was accompanied by local transition of rifting to spreading and partial rupture of the continental lithosphere, in particular, within the Kainuu Belt along the boundary between the Kuhmo–Segozero and Kianta GGDs (Fig. 2, *b*). The Jormua ophiolite complex retained in the present-day structure marks the rupture of the continental crust ~1.95 Ga ago and short-term existence of the oceanic structure of the Red Sea type [*Peltonen et al., 1998*]. The spatial distribution of Palaeoproterozoic mafic–ultramafic igneous rocks and the lower crustal reflectivity zone in the seismic images of the crust along the CMP seismic profiles allows us to consider the reflectivity zone as a manifestation of underplating [*Mints, 2011; Thybo, Artemieva, 2013, and references therein*].

In the Late Palaeoproterozoic history of the composite East European Craton, the final event was formation of the arcuate intracontinental Lapland–Mid-Russia–South Baltia Collisional Orogen that surrounds the Karelian Craton in north, east, south, and southwest and the Svecofennian Orogen along the western margin of the Karelian Orogen 1.93–1.87 Ga ago [*Mints et al., 2015; Mints, 2011*]. The evolution of the Svecofennian paleoocean was completed by eastward subduction of the oceanic lithosphere and accretion of island-arc complexes and rocks of inter-arc basins to the margin of the Karelian Craton. In the course of accretion, most of these complexes were thrust under the continental margin, whereas others, conversely, were thrust over the margin. These movements resulted in the formation of a crocodile-type structure [*Abramovitz et al., 1997; Mints et al., 2009*] that is characteristic of marginal continental and collisional orogens. Scrutiny of the seismic crustal image along the FIRE-1 profile [*Kukkonen, Lahtinen, 2006*] makes it possible to trace tectonic sheets composed of accreted volcanic–plutonic complexes beneath the Archaean crust of the Karelian Craton.

The thrust–nappe ensembles of granulite-gneiss belts were formed by ~1.87 Ga in the setting of overall collisional compression. The tectonic sheets making up the South Finland Belt were thrust from the south over the Svecofennian Orogen almost immediately after its formation [*Mints et al., 2015*]. These events completed the Palaeoproterozoic history.

A new stage in evolution of the crust (the last in the considered time interval) was related to formation of the Mesoproterozoic rapakivi granite pluton in the eastern part of the Russain Platform. The 3D model of deep structure of the Early Precambrian crust based on geological evidence and interpretation of CMP seismic profiles demonstrates an image of the tectonically delaminated crust with predominance of low-angle boundaries between the main tectonic units and shows complex structure of the crust–mantle boundary [*Mints, 2011*].

4. Complex geophysical model

The complex interpretation of gravimetric and geothermal data is based on the results of regional seismic DSS studies and CMP profiling of the sedimentary cover of the adjacent platform, as well as seismic estimation of the crust thickness. This heterogeneous information described in [*Glaznev, 2003; Grad et al., 2009*] were used for creation of the initial seismogeological model of the crust for the territory much larger than the area of the eventual 3D complex model of the lithosphere (Fig. 3) in order to take into account the influence of marginal zones when solving direct and inverse problems related to thermal and density simulation.

Statistical analysis of the seismic data allowed us to recognize four layers with characteristic velocities, which correspond to the integrated models of the continental crust [*Christensen, Mooney, 1995*]. The estimates of the total thickness of the crust based on CMP profiling, which generally coincide with results of DSS

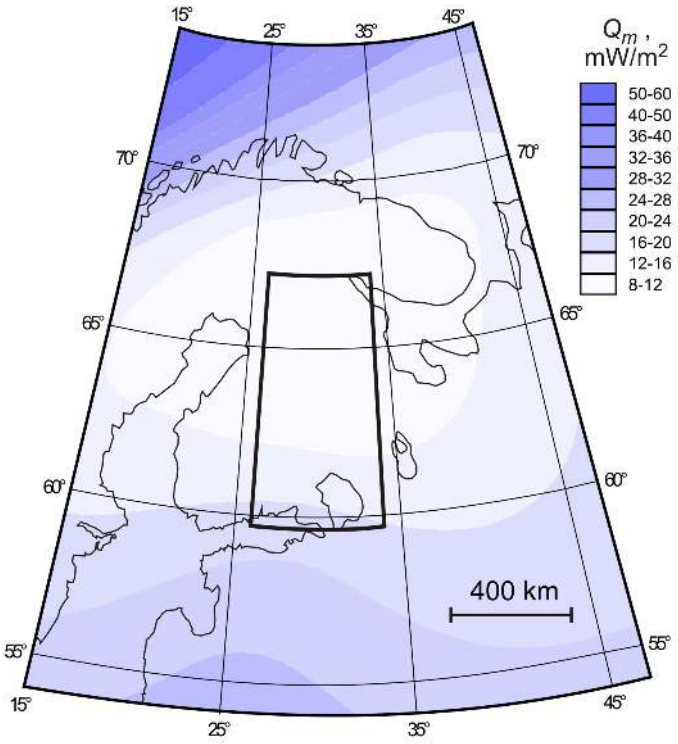

Fig. 3. Smoothed mantle heat flow in the eastern Fennoscandian Shield and the adjacent part of the Russian Plate. The area of simulation is shown.

Рис. 3. Схема сглаженного мантийного теплового потока (в мВт/м²) для восточной части Фенноскандинавского щита и сопредельной части Русской платформы. Показан контур результативной области моделирования.

[*Berzin et al., 2002*], were also used as initial data for complex geophysical simulation.

4.1. Thermal model of the Earth's crust and upper mantle

At the first stage of simulation, the 3D stationary thermal model of the lithosphere is created on the basis of the data on the regional surface heat flow, thermal conductivity and heat generation in the crust [*Glaznev, 2003*], according to the initial seismogeological model of the crust, and the data on the upper mantle of the studied region. The 3D thermal model is calculated in spherical coordinates with spacing of 0.25° in latitude, 0.5° in longitude, and 5 km along radius down to a depth of 65 km. The model combines distribution of temperature and heat generation in the Earth's crust plus estimation of the deep (mantle) heat flow currently supplied from the mantle to the lower edge of the model.

The mantle-derived heat flow appreciably affects temperature distribution in the studied medium. Therefore, estimation of this boundary condition is crucial for all the subsequent procedures developing of the model. The initial data used for estimation of the mantle heat flow are based on the classification of the studied territory by thickness of crustal layers, which was carried out on the basis of the seismogeological model of the region. As a result, the region is subdivided into a number of large blocks, each having its relatively homogeneous seismic structure, and the mantle heat flow is estimated for each of the blocks [*Glaznev, 2003*].

The smoothed calculated values of the mantle heat flow (Fig. 3) are consistent with the estimates previously obtained for particular areas of the Fennoscandian Shield [*Balling, 1995; Pasquale et al., 1991*]. These values make it possible to differentiate the recent thermal activity of the mantle. The lowest mantle heat flow values (no higher than 8–10 mW/m²) are estimated for the Karelian Craton, the Belomorian and Kola Provinces, which are typical of domains that underwent the Archaean consolidation [*Nyblade, Pollack, 1993*]. The low mantle heat flow in these areas was partly caused by the effect of paleoclimatic processes on the recent surface heat flow [*Kukkonen et al., 1998; Glaznev et al., 2004*]. In the adjacent Russian Platform and the Barents Sea Plate that were also impacted by the last glaciation, the minimum mantle heat flow is evidently local against the background of relatively high values (up to 16÷24 mW/m²) and probably reflects a level of recent thermal activity of the upper mantle in the eastern Fennoscandian Shield.

Based on the solution of the 3D inverse problem of geothermics in the setting (Eqs. 2, 4, 6, 8, 10) with an allowance for the estimated mantle heat flow, a correct stationary temperature model of the medium is created. A discrepancy of the eventual thermal model (Eq. 2) is ±3.7 mW/m², and this value is commensurable with the uncertainty of the initial geothermal data. For the deep levels, the accuracy of temperature calculation from the stochastic simulation results is estimated at ±40 °C.

Temperature values at various depth levels of the 3D model are shown in Fig. 4. The temperature distribution pattern in the crust demonstrates an isometric area of relatively low temperatures in the northern Karelian Craton and the southwestern Belomorian Province. Along with relatively homogeneous distribution of radiogenic chemical elements in the Earth's crust [*Glaznev, Skopenko, 1991*], such an anomalous temperature area is indicative of the heterogeneous mantle heat flow in the crust of the region. A potential increase in the horizontal temperature gradient is revealed at the lower levels of the thermal model (40–60 km) in the southwestern part of the studied region; it may be caused by substantially increased surface and mantle heat flows in the zone of transition to the South Baltica segment of the intracontinental Late Palaeoproterozoic

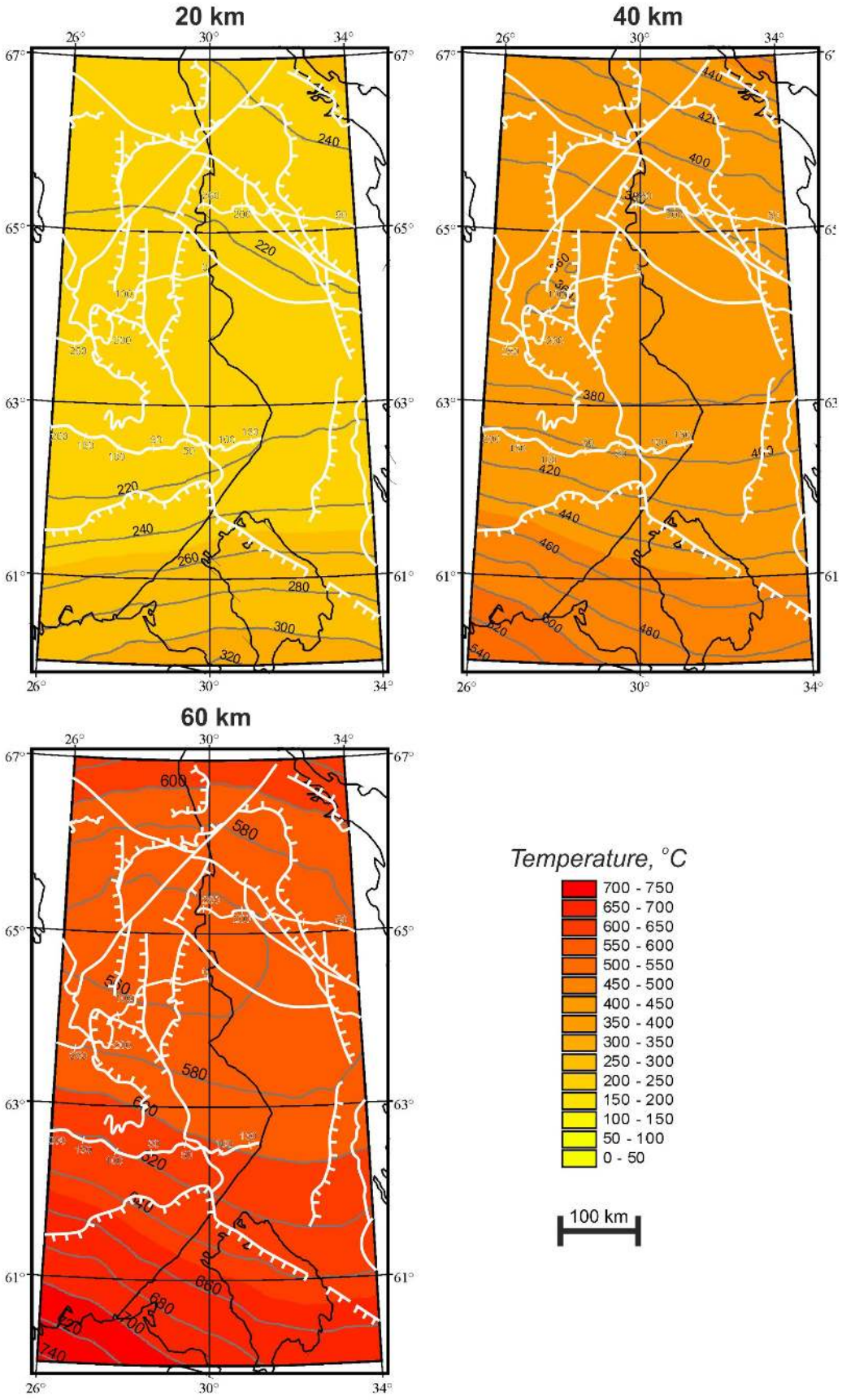

Fig. 4. Temperature distribution in the Earth's crust at depths of 20, 40, and 60 km. In Figs. 4–7 and 12, white lines show contours of geological structures at the surface and seismic CMP profiles (see Fig. 2).

Рис. 4. Распределение температур в земной коре на глубинах 20, 40 и 60 км (в °С). На рис. 4–7 и 12 белыми линиями показаны контуры геологических структур на дневной поверхности и профилей МОГТ, представленных на рис. 2.

Lapland–Mid-Russia–South Baltica Collisional Orogen overlain by the sedimentary cover of the Russian Platform [*Mints et al., 2015; Mints, 2011*]. The map of the surface heat flow in Europe [*Artemieva et al., 2006*] (Fig. 3) shows similar regular patterns of heat flow distribution in the Karelian Craton and the surrounding arcuate orogen at the regional level.

The 3D model of temperature distribution is a necessary element of the complex velocity–density model of the crust, which provides insights into the nature of deep-seated geophysical boundaries.

4.2. Density model of the Earth's crust and upper mantle

At the second stage of simulation, an initial density model of the crust is created on the basis of velocity and thermal models. Validation with gravity data makes it possible to estimate discrepancy between the observed gravity field and the estimated effect of the initial model. The direct problem for the upper crust is solved with account of the available data on density of the near-surface rocks in the studied region [*Galitchanina et al., 1995*] and stochastic estimations of thickness of the 'gravity active layer' in the range from 2.5 to 14 km [*Glaznev, 2003*]. When the gravity field is computed from the initial approximation, densities of the near-surface rocks are extrapolated only over the gravity active layer, while densities corresponding to the initial velocity model are taken into account for the deeper layers. Such an approach is dictated by the necessity to take into account, at least, roughly the data on shallow-seated rock complexes in initial approximation of the model, and specific features of such an approach make a certain impact on the resultant density model (this issue is discussed below).

For solving direct and inverse problems of gravimetry, the planetary density model of the Earth's crust and its gravity field [*Kartvelishvili, 1983*] is used as a normal density model. Our model is based on the solution of the inverse 3D problem of gravimetry in the spherical setting with account of the actual topography. The initial data include the difference gravity field of initial approximation of the model and the initial density model of the crust. The network 0.25° in latitude, 0.25° in longitude, and 5 km in depth is used in solution of inverse problem. The eventual discrepancy of density model determined by Eq. 1 is ±2.4 mGal. The accuracy of calculated density in network elements of model is ±0.02 g/cm^3.

The eventual density model is isostatically compensated owing to special constraints placed into the algorithm of inverse problem solution, which ensure the absence of significant mass forces at the lower edge of model. The final 3D density model is presented in Figs. 5–7 as a series of horizontal slices.

It has been repeatedly shown that the crust models characterizing distribution of P-wave velocities correspond to density layering of the crust. The boundaries of layers are fragmentary fixed by abrupt variations of velocity and density. With rare exception, these parameters regularly increase with depth and from top to bottom of particular layers [*Christensen, Mooney, 1995; Korsman et al., 1999; Kuusisto et al., 2006*]. The obtained model also demonstrates that density of the crust increases with depth, however, the layer boundaries remain vague.

At the uppermost level of the model (Fig. 5), the density of rocks is 2.52–2.88 g/cm^3 (2.69 g/cm^3, on average). These values are consistent with the regional petrophysical data [*Galitchanina et al., 1995*]. Against the background of the average values, clearly detectable are anomalies caused by the presence of high-density gabbroanorthosites and granulites of the Kolvitsa–Umba Belt, layered mafic–ultramafic intrusions, the Palaeoproterozoic volcanic–sedimentary and the Archaean greenstone belts. Anomalies related to the rocks of the Svecofennian accretionary complex are not so contrasting. It should be noted that configurations and sizes of the high-density anomalies are mainly associated with the initial density model as objects smaller than 20–25 km cannot be reliably reflected in its discrete representation within the given network. Nevertheless, a certain increase in density is revealed for narrow, sufficiently long high-density objects.

Low-density anomalies at the upper level of the model reliably mark the spatial position of rapakivi granite in the southeast and granitic rocks of the Central Lapland Complex in the northwest. The area of the lower density in the southeast corresponds to the platform sedimentary cover and partly to rapakivi granite.

At depths of 5–10 km, which, in fact, are near-surface and occupy two upper layers in the model network, density varies from 2.62 to 2.88 g/cm^3 (2.75 g/cm^3 on average). The domain of elevated values up to 2.82–2.86 g/cm^3 is located in the southwestern Karelian Craton and the adjacent Svecofennian Orogen. In contrast, the eastern Karelian region at depths of 5–10 km differs in lower density (up to 2.68–2.72 g/cm^3). The low-density crust apparently underlies Palaeoproterozoic volcanic–sedimentary belts. Large dimensions of the anomaly with relatively low density give evidence of its existence in reality and reflect internal features of the upper crust of the Karelian Craton. With sinking to deeper levels, the density contour lines shift to the east, indicating a gentle slope of isodensity surfaces in the eastern and northeastern directions.

It is noteworthy that a negative anomaly of density at depths of 5–10 km is located near the northern boundary of the model beneath the central part of the Palaeoproterozoic Kuolajärvi structure (Fig. 2, *b*) filled largely with mafic metavolcanics. It is suggested that this anomaly is compensating, i.e. arising by solution of

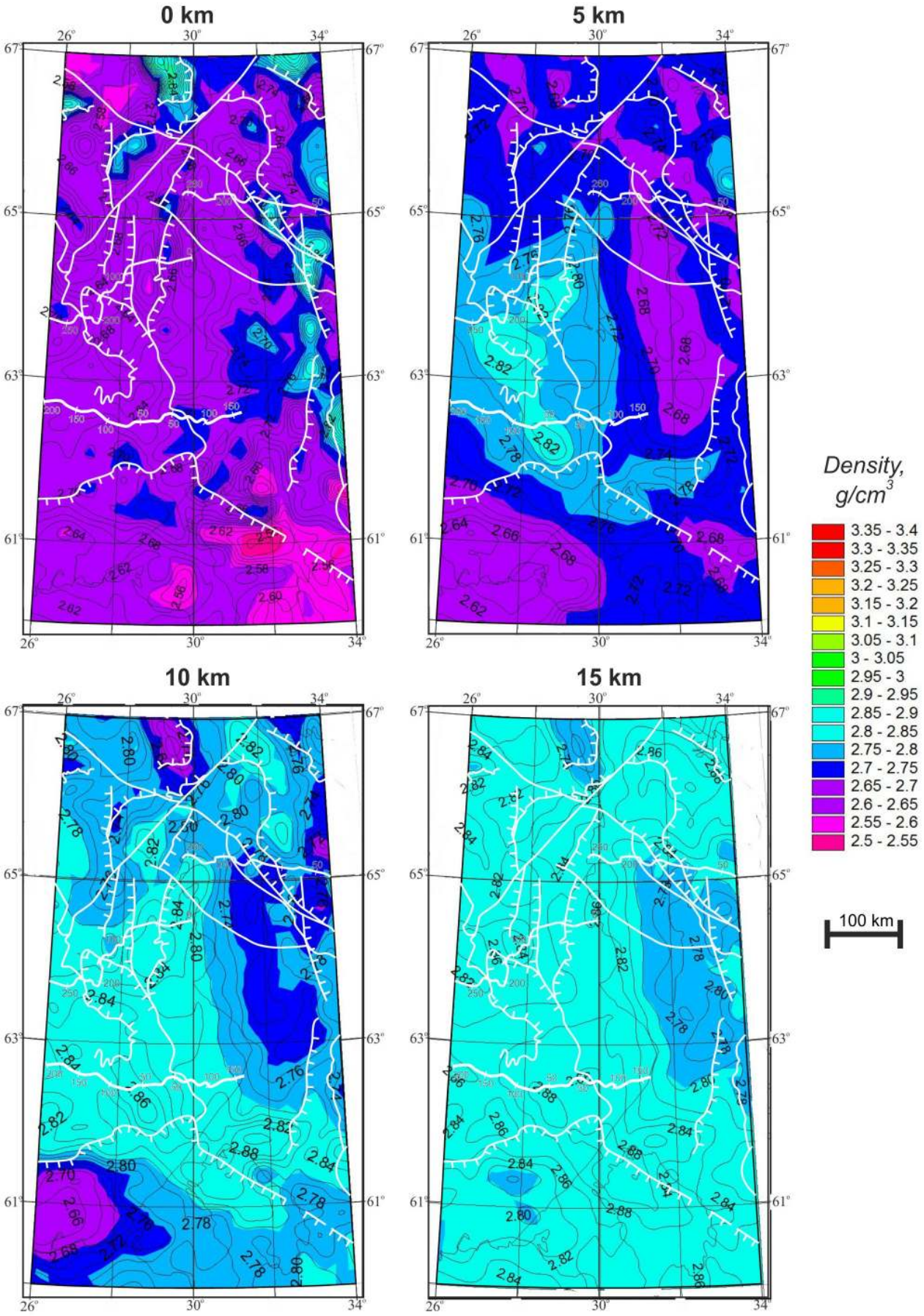

Fig. 5. Density distribution in the Earth's crust at depths of 0, 5, 10, and 15 km.

Рис. 5. Распределение плотности в земной коре на глубинах 0, 5, 10 и 15 км (значения плотности в г/см^3).

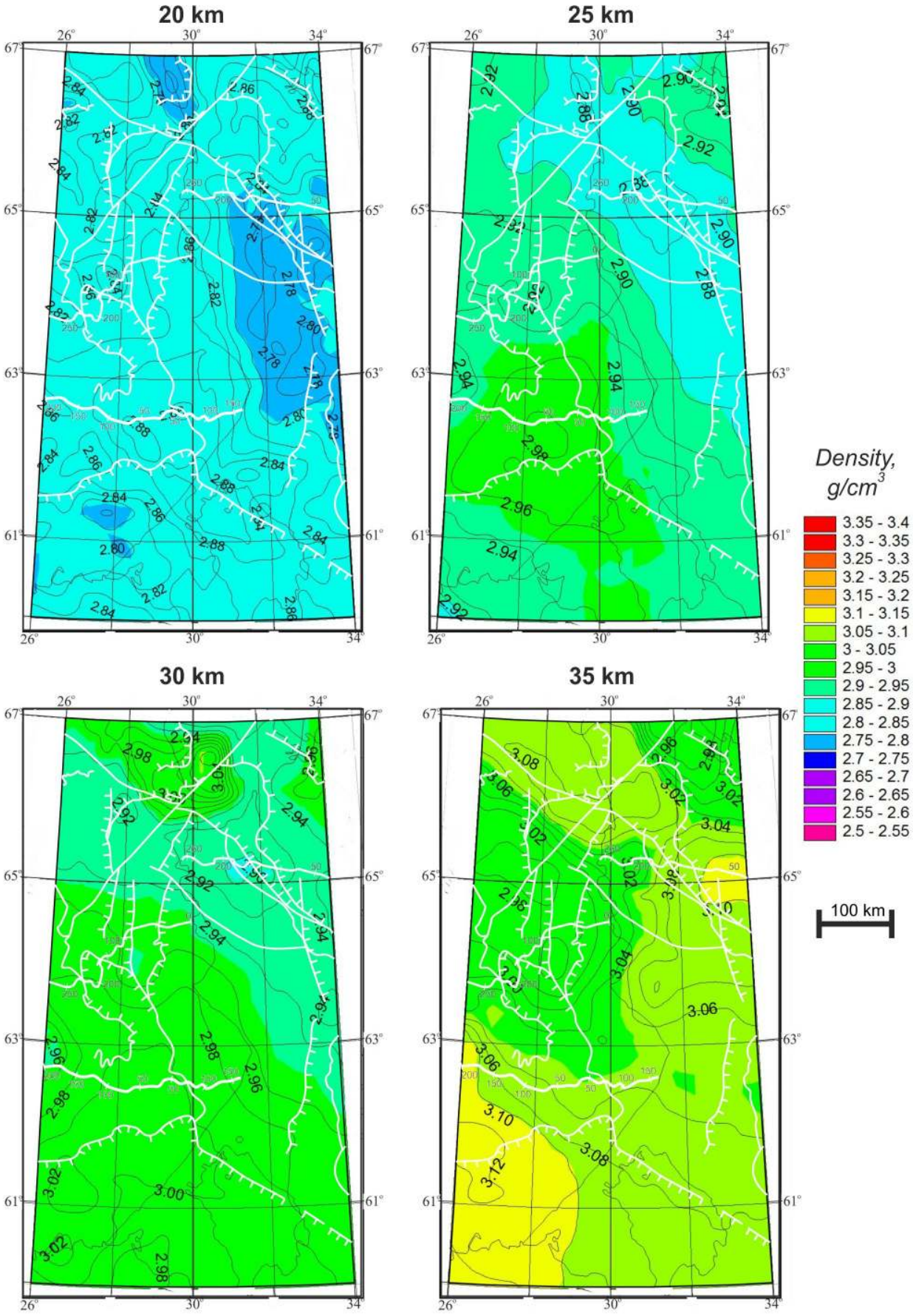

Fig. 6. Density distribution in the Earth's crust at depths of 20, 25, 30, and 35 km.

Рис. 6. Распределение плотности в земной коре на глубинах 20, 25, 30 и 35 км (значения плотности в г/см^3).

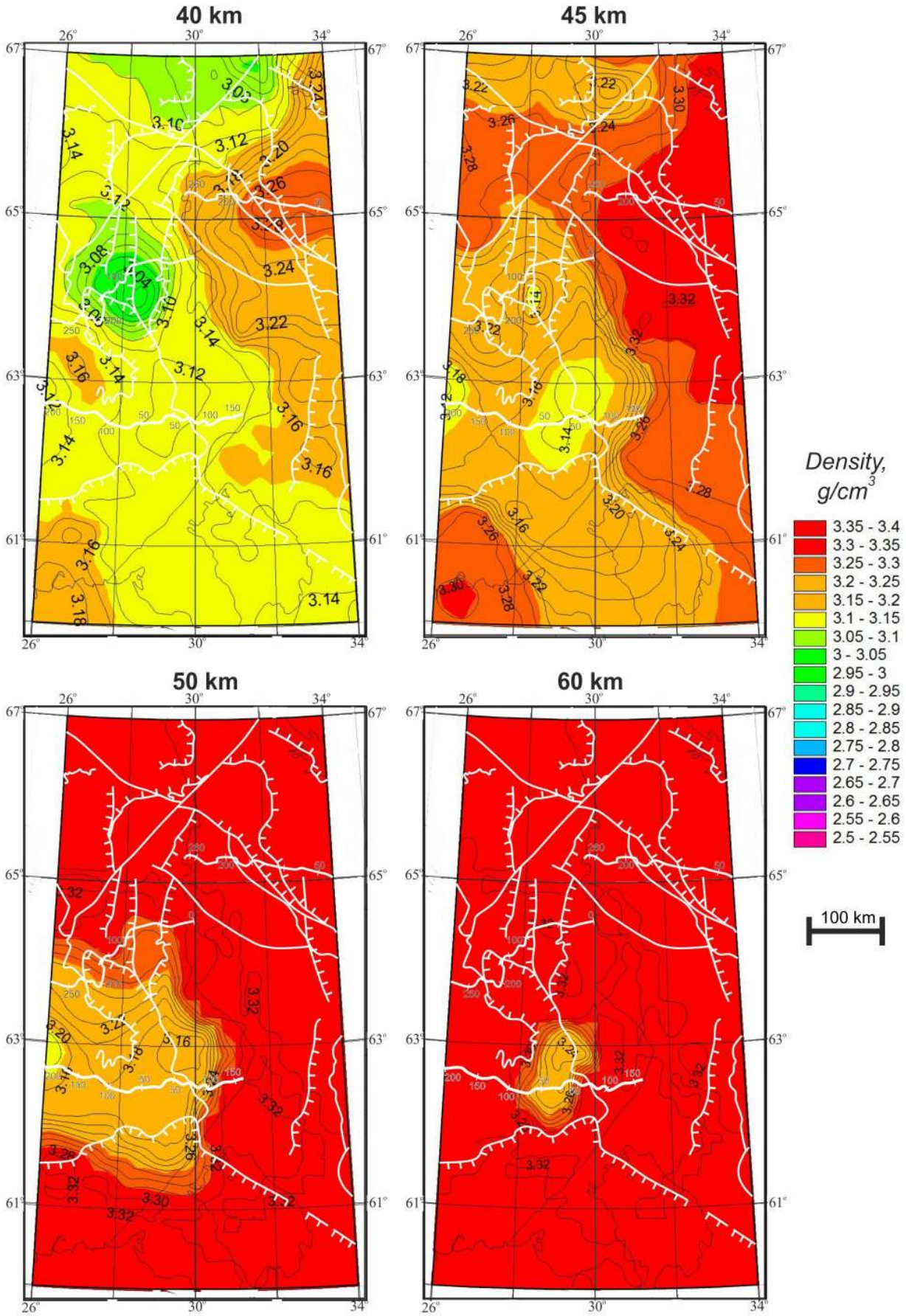

Fig. 7. Density distribution in the Earth's crust at depths of 40, 45, 50, and 60 km.

Рис. 7. Распределение плотности в земной коре на глубинах 40, 45, 50 и 60 км (значения плотности в г/см^3).

the inverse problem of gravimetry as a result of overestimation of thickness of the volcanic–sedimentary complex in the initial density model. The vertical section of the Kuolajärvi structure is apparently smaller than its estimate from the averaged thickness of the gravity active layer, and the total vertical thickness of metavolcanic rocks does not exceed 2–3 km.

In the southwestern part of the region, an anomaly of relatively low density (2.60–2.68 g/cm^3) is distinctly revealed at the same depth in the upper crust. This anomaly is related to the deep portion of the Wyborg rapakivi granite pluton (Fig. 2, *b*).

The upper crust at depths of 15–20 km is distinguished by relatively weak differentiation of the medium in the lateral direction within a density range of 2.78 to 2.92 g/cm^3. The vertical gradient of rock density is also insignificant. At the levels of 15 and 20 km, the average density is 2.83 and 2.87 g/cm^3, respectively. Nevertheless, the crust density of the Karelian Craton decreases from the southwest to the northeast. This is especially appreciable at the level of 20 km, where relatively low-density rocks occupy almost the entire area of the Karelian Craton. The rocks of relatively elevated density in the west are related to the Svecofennian Orogen.

In the middle crust of the Karelian Craton at depth levels of 25 and 30 km (Fig. 6), the rock density varies from 2.88 to 3.04 g/cm^3 with a tendency to decrease in the northeastern direction to 2.88–2.94 g/cm^3. The rocks of the Belomorian Province adjoining the Karelian Craton in the east are characterized by increase in density up to 2.96–3.02 g/cm^3. In general, the distribution of density at depths of 25–30 km suggests that the contour lines of rock density at 2.93–2.95 g/cm^3 beneath the central part of the Karelian Craton depict the eastern boundary of the Svecofennian Orogen plunging eastward.

At the level of the lower crust (35–45 km), rock densities vary within a range of 2.98–3.26 g/cm^3 (Figs. 6, 7). The highest density values are characteristic of the transitional crust–mantle zone approximately at the level of Moho discontinuity. The density model of the lower crust is distinguished by an anomalous domain of low density (2.98–3.02 g/cm^3) at a depth of 35 km beneath the western part of the Karelian Craton. At the level of 40 km, this anomaly is significantly reduced in dimensions. Similar relationships are also noted at deeper slices of the model and thus bear systematic character.

In the lowermost crust at depths of 40–45 km (Fig. 7), the rocks with density ranging from 3.10 to 3.30 g/cm^3 are related to the transitional crust–mantle zone (crust–mantle mixture?). At depths of 50–60 km, the mantle rocks occupy almost the entire domain of simulation. The only exception is the region of the anomalously deep Moho discontinuity at the boundary between the Karelian Craton and the Svecofennian Orogen [*Grad et al., 2009; Kozlovskaya et al., 2004*].

The vertical step of the network is 5 km in the accepted discretization of the model and thus does not allow us to determine unambiguously a position of the Moho boundary. Densities exceeding 3.30 g/cm^3 are reliably related to the mantle rocks, whereas densities below 3.20 g/cm^3 are typical of the lowermost crustal rocks. The density of 3.24 g/cm^3 approximately corresponds to the Moho discontinuity. The contour lines of this density depict a surface, which coincides with the Moho discontinuity interpolated on the basis of the initial seismic data. The calculated average depths are 45.5 and 45.3 km, respectively, and the mean square difference of these depths (±2.1 km) is minimal as compared with all other isodensity surfaces. The obtained mean square discrepancy corresponds to accuracy of initial data on the Moho depth in the studied region [*Grad et al., 2009*] and allows us to consider the isodensity surface of 3.24 g/cm^3 as an analog of Moho discontinuity in the density model (velocity–density Moho discontinuity). The use of this image of Moho discontinuity coinciding in accuracy with the DSS data seems to be more correct, because the density model is fully agreed with the observed gravity field. A maximal discrepancy between depths of the isodensity surface and the seismic Moho boundary exceeding 4 km is noted in the southeastern region of simulation, where DSS data are absent and the initial seismogeological model of the crust was created as interpolation of the data on converted waves [*Sharov et al., 2005*] of low accuracy.

The depth and topography of the velocity–density Moho discontinuity are shown in Fig. 8, where the isodensity surface of 2.9 g/cm^3 is also given for comparison. The relationship of the depths of these boundaries demonstrates an approximate isostatic compensation of the density model: decrease in thickness of the upper low-density part of the Earth's crust is compensated by significant increase in thickness of the lower high-density part of the crust. In the domain of the anomalously deep position of the velocity–density Moho discontinuity at a depth of ~63 km, the compensation is partly supplemented by increase in density of the lowermost Earth's crust (Fig. 7). The plunging velocity–density Moho discontinuity (Fig. 8) is spatially coincident with a «Moho depression» earlier recognized on the basis of seismic data and density simulation [*Kozlovskaya et al., 2004*].

5. Deep structure: Geological model based on interpretation of seismic crustal images in sections along CMP seismic profiles

Information on deep geological structure of the region is based on results of geological mapping and

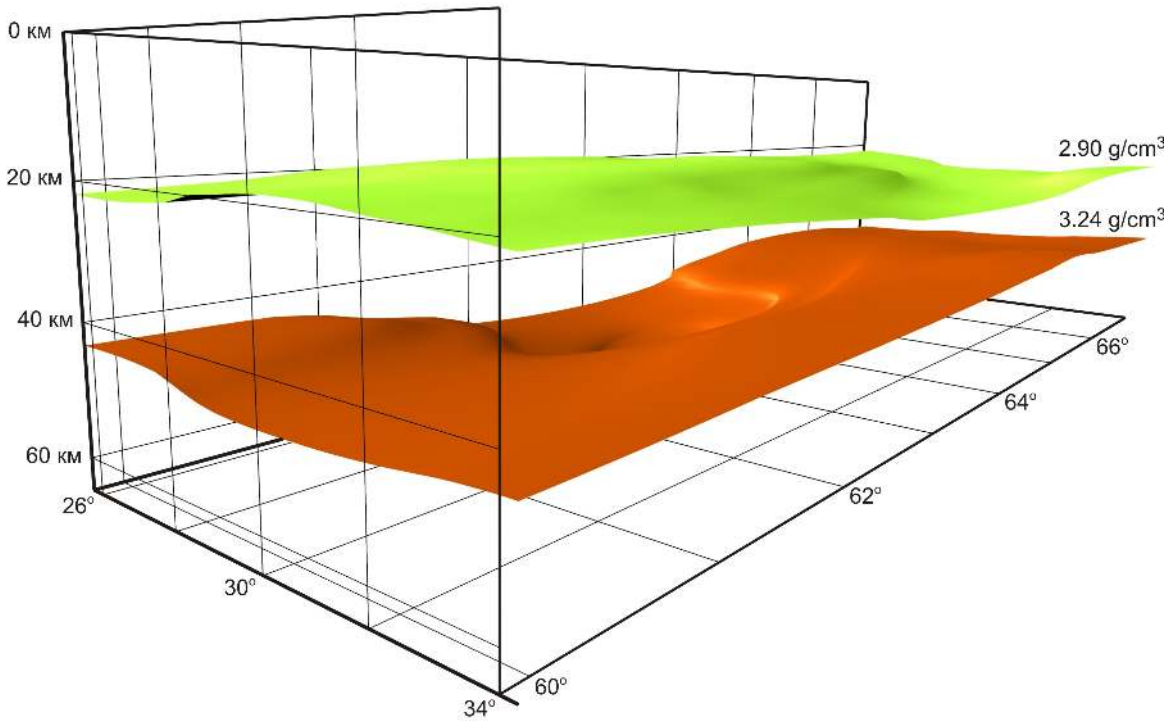

Fig. 8. Smoothed isodensity surfaces separating the middle and lower crust (2.90 g/cm^3), the lower crust and the upper mantle (3.24 g/cm^3), and the velocity–density Moho discontinuity.

Рис. 8. Положение и морфология сглаженных изоплотностных поверхностей, разделяющих: 2.90 г/см^3 – среднюю и нижнюю кору, 3.24 г/см^3 – нижнюю кору и мантию (сейсмоплотностной раздел Мохо).

studies along CMP seismic profiles: 4B (Fig. 9), FIRE-1 (Fig. 10), and FIRE-3-3A (Fig. 11) [*Kukkonen, Lahtinen, 2006; Mints et al., 2009, 2015; Mints, 2011*].

Careful correlation of geological structural units at the surface and geological interpretation of seismic crustal images along 1-EU and 4B CMP profiles has provided for creation of a 3D model of geological structure of the crust and upper mantle in the studied region. The geological interpretation of seismic images of the crust along the FIRE-1 and FIRE-3-3A profiles in Finland carried out by M.V. Mints serves as an additional support of the western part of the 3D model and allows us to provide insights into the structure of the Svecofennian Orogen and to characterize its boundary with the Karelian Craton [*Mints et al., 2009, 2015*].

5.1. Archaean tectonic units

In the vertical section along 4B profile (Fig. 9), the sheet-like wedge-shaped domain represents the Archaean granite–greenstone crust of the Kuhmo–Segozero microcontinent , which is the main constituent of the Karelian Craton. The maximum thickness of the sheet amounts to almost 30 km near the western and southwestern margins of the microcontinent, and the sheet gradually becomes thinner while plunging eastward beneath the Khetolambina microcontinent. The southeastern margin of the Kuhmo–Segozero microcontinent plunges beneath the Vodlozero microcontinent. The section along 4B profile indicates that the tectonic sheet of Kuhmo–Segozero microcontinent overlying the lower crust underwent tectonic displacements and became slanted after formation of isometric acoustically transparent domains, i.e. large granitic plutons in our interpretation. Their formation can be logically attributed to the completion of the Neoarchaean evolution.

5.2. Palaeoproterozoic tectonic units

The boundary zone of the Lapland sector of the Palaeoproterozoic intracontinental orogen is located at the eastern part of the studied region, which is intersected by 4B profile. This zone is represented by the structural ensemble of the imbricate East Karelian Thrust Belt composed of alternating tectonic sheets of the Archaean granite–greenstone and Palaeoproterozoic volcanic–sedimentary associations.

The lower crustal layer with intense seismic reflections stands out at the base of the Karelian Craton. The overlying gently dipping geological bodies gradually flatten when approaching the upper boundary of this

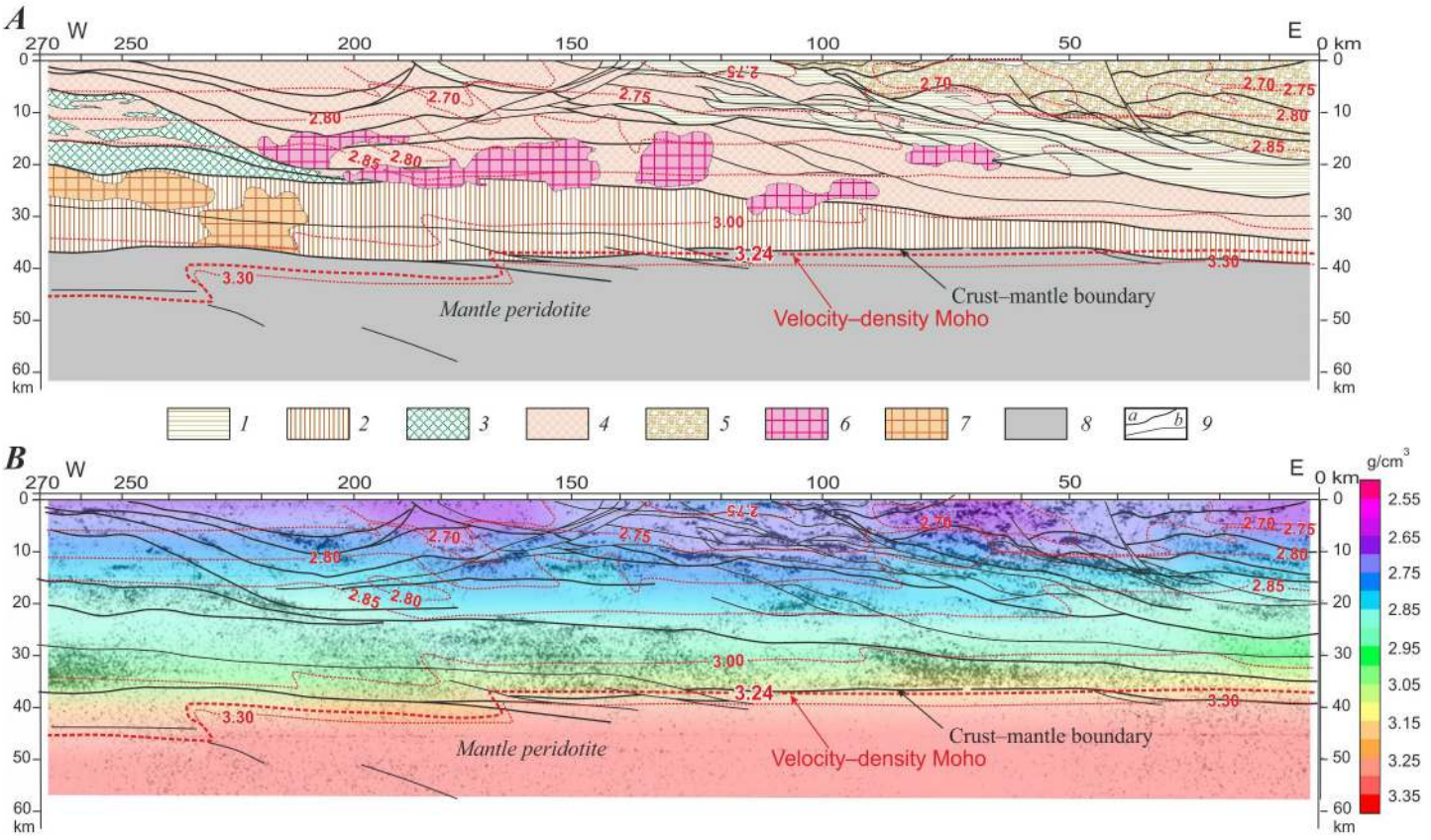

Fig. 9. Sections of the crust and the upper mantle along 4B profile: (*A*) geological section obtained as a result of geological interpretation of the seismic crustal image [*Mints et al., 2009, 2015*]; (*B*) density section (section of 3D crust model). Main tectonic boundaries and certain isodensity contours (including the velocity–density Moho discontinuity, 3.24 g/cm^3) are shown.

1–2 – Palaeoproterozoic: *1* – volcanic–sedimentary belt, *2* – lower crustal granulite-basic complex; *3–5* – Archaean: *3* – rocks of greenstone belts, mainly basic volcanics, *4* – Kuhmo–Segozero TTG gneiss complex with inclusions of metavolcanic and metasedimentary rocks, *5* – Khetolambina granite–greenstone complex; *6–7* – plutons: *6* – in the middle crust, mainly granitoids, *7* – in the lower crust, mainly gabbro and gabbroanorthosite; *8* – mantle peridotite; *9* – faults, mainly of reverse–thrust type: (*a*) major and (*b*) subordinate.

Рис. 9. Разрезы коры и верхней части мантии по профилю 4В: (*A*) геологический, полученный в результате геологической интерпретации сейсмического образа коры [*Mints et al., 2009, 2015*]; (*B*) плотностной – сечение трехмерной модели коры; показаны главные тектонические границы и некоторые изолинии плотности (в том числе сейсмоплотностной Мохо – 3.24 г/см^3).

1–2 – палеопротерозой: *1* – осадочно-вулканогенные пояса, *2* – гранулит-базитовый комплекс пород нижней коры; *3–5* – архей: *3* – породы зеленокаменных поясов, преимущественно вулканиты основного состава, *4* – Кухмо-Сегозерский гранитогнейсовый комплекс с включениями метавулканитов и метаосадков, *5* – Хетоламбинский гранит-зеленокаменный комплекс; *6–7* – плутоны: *6* – в средней коре, предположительно гранитоиды, *7* – в нижней коре, предположительно габбро и габбро-анортозиты; *8* – мантия (мантийные перидотиты); *9* – разломы, преимущественно взбросо-надвигового типа: главные (*a*) и второстепенные (*b*).

layer. The determinant role in origin and composition of this layer belongs to the Palaeoproterozoic under- and intraplating by the mantle-derived mafic magmas, which underlie the Archaean crust of the Karelian Craton [*Kempton et al., 2001; Mints et al., 2009, 2015; Mints, 2011, and references therein*].

In the southwestern part of the region crossed by FIRE-1 and FIRE-3-3A profiles, tectonic sheets composed of island-arc and back-arc complexes of the Svecofennian Orogen are traced from the surface to the crust–mantle boundary and plunge further as if «dissolving» in the mantle. The total thickness of the accretionary complex exceeds 30 km. As shown in the geological section along FIRE-1 seismic profile (Fig. 10), starting from stake 230 km and further southeastward, the profile crosses the Svecofennian Orogen and Central Finland granitoid pluton, one of the largest in the Fennoscandian Shield. It is evident from the seismic profile that this pluton is a nearly horizontal layered sheet, which maximum thickness does not exceed

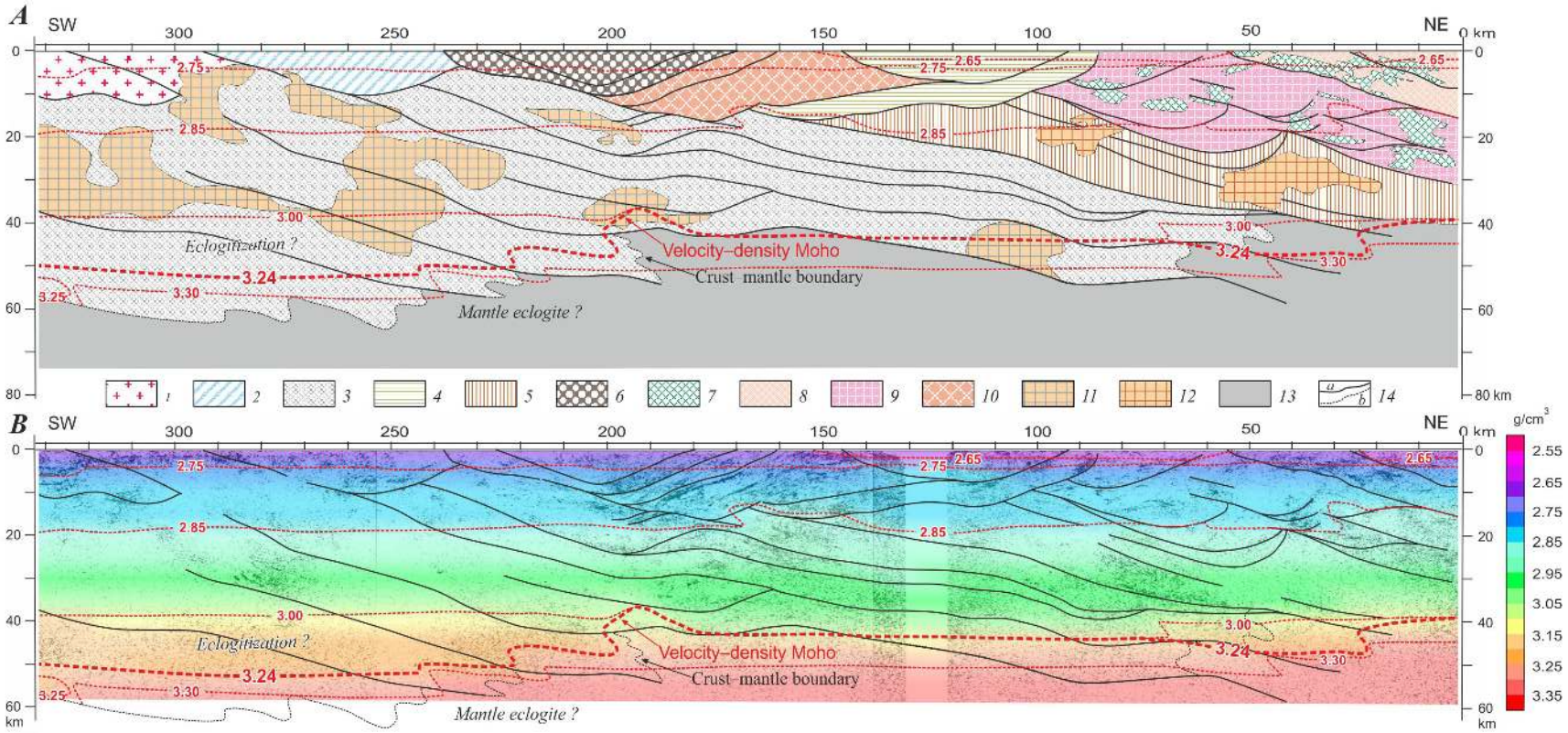

Fig. 10. Sections of the crust and the upper mantle along FIRE-1 profile: (*A*) geological section obtained as a result of geological interpretation of the seismic crustal image [*Mints et al., 2015*]; (*B*) density section (section of 3D crust model). Main tectonic boundaries and certain isodensity contours (including the velocity–density Moho discontinuity, 3.24 g/cm^3) are shown.

1–5 – Palaeoproterozoic: *1–3* – Svecofennian Orogen: *1* – granitoids of Central Finland pluton, *2* – Savo Accretionary Belt, *3* – tectonic sheets overlain by granitoids of Central Finland pluton, *4* – volcanic–sedimentary complex of Kainuu Belt, *5* – lower crustal granulite-basic complex; *6–9* – Archaean: *6* – Varpaisjärvi granulite-gneiss complex, including diaphtorites, *7* – rocks of greenstobe belts, mainly basic volcanics, *8* – Kuhmo–Segozero, *9* – Kjanta, *10* – Iisalmi TTG complex; *11–12* – plutons: *11* – presumably granitoids in accretionary complex, *12* – presumably gabbro and gabbroanorthosite in Palaeoproterozoic lower crustal complex; *13* – mantle rocks with significant or predominant participation of eclogites; *14* – geological boundaries: (*a*) reverse–thrust and over- and underthrust faults, (*b*) diffuse crust–mantle boundary.

Рис. 10. Разрезы коры и верхней части мантии по профилю FIRE-1: (*A*) геологический, полученный в результате геологической интерпретации сейсмического образа коры [*Mints et al., 2015*]; (*B*) плотностной – сечение трёхмерной модели коры; показаны главные тектонические границы и некоторые изолинии плотности (в том числе сейсмоплотностной Мохо – 3.24 г/см^3).

1–5 – палеопротерозой: *1–3* – Свекофеннский аккреционный ороген: *1* – гранитоиды Центрально-Финляндского плутона, *2–3* – аккреционный комплекс: пояс Саво (*2*), тектонические пластины, перекрытые гранитоидами Центрально-Финляндского плутона, погружающиеся под окраину Карельского кратона (*3*), *4* – осадочно-вулканогенный комплекс пояса Кайнуу, *5* – гранулит-базитовый комплекс пород нижней коры; *6–9* – архей: *6* – гранулито-гнейсовый комплекс Варпаисъярви (в том числе диафторированные разности гранулитов), *7* – породы зеленокаменных поясов, преимущественно вулканиты основного состава, *8–10* – гранитогнейсовые комплексы: Кухмо-Сегозерский (*8*), Кьянта (*9*), Рануа-Иисалми (*10*); *11–12* – плутоны: *11* – в аккреционном комплексе, предположительно гранитоиды, *12* – в палеопротерозойском нижнекоровом комплексе, предположительно габбро и габбро-анортозиты; *13* – мантия (предположительно со значительным или преобладающим участием эклогитов); *14* – главные геологические границы: разломы, преимущественно взбросо-надвигового и надвиго-поддвигового типа (*a*), диффузная граница между корой и мантией (*b*).

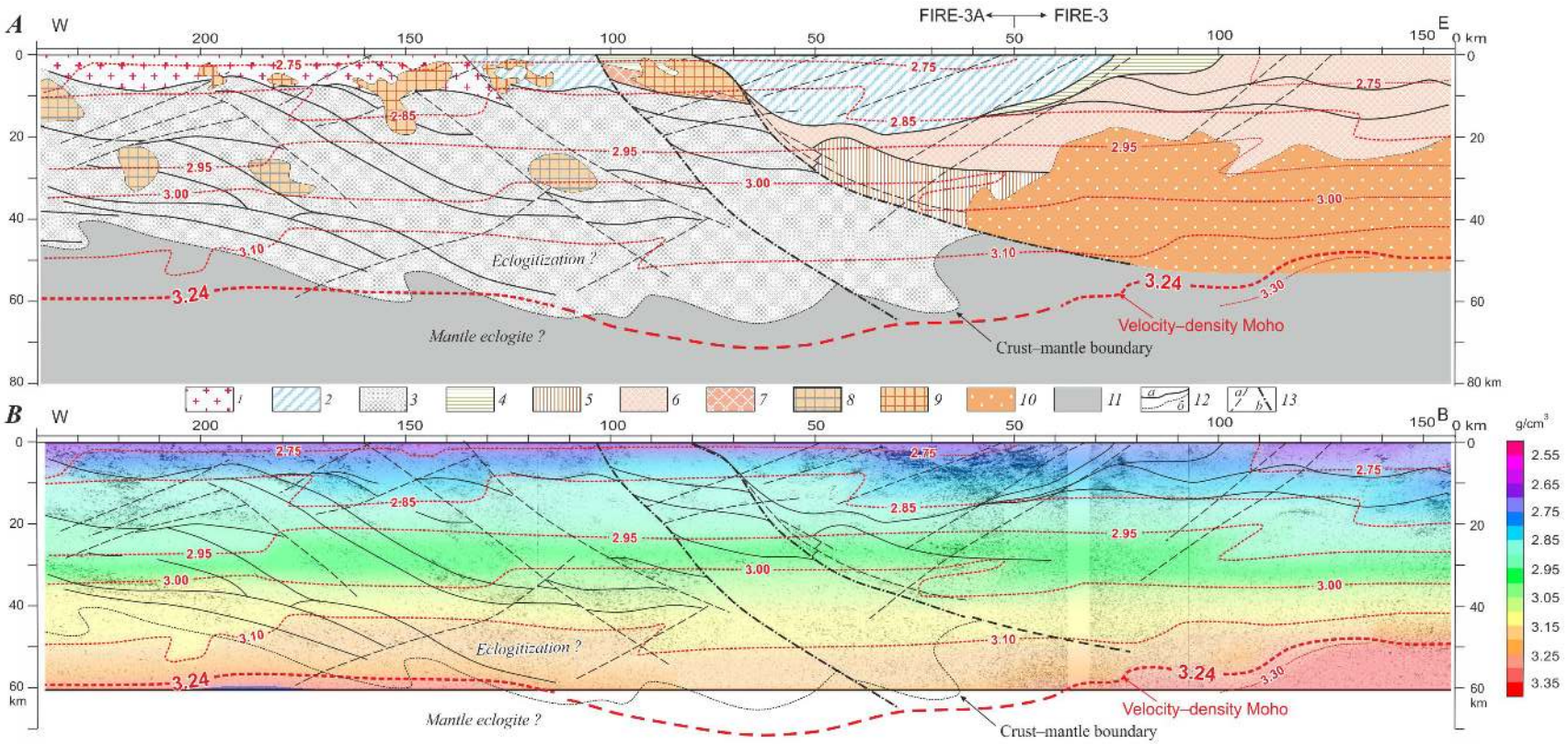

Fig. 11. Sections of the crust and the upper mantle along FIRE-3-3A profile: (*A*) geological section obtained as a result of geological interpretation of the seismic crustal image; (*B*) density section (section of the 3D crust model). Main tectonic boundaries and certain isodensity contours (including the velocity–density Moho discontinuity, 3.24 g/cm^3) are shown.

1–5 – Palaeoproterozoic: *1–3* – Svecofennian Orogen: *1* – granitoids of Central Finland pluton, *2* – Saimaa Accretionary Belt, *3* – tectonic sheets plunging beneath margin of Karelian Craton and overlain by granitoids of Central Finland pluton, *4* – volcanic–sedimentary complex of passive margin, *5* – lower crustal granulite-basic complex; *6–9* – Archaean: *6* – Kuhmo–Segozero and *7* – Iisalmi TTG gneiss complex; *8–9* – plutons presumably granitoid in accretionary complex (*8*) and upper crust (9); *10* – acoustically transparent domain in middle–lower crust presumably homogenized as a result of high-temperature metamorphism; *11* – mantle rocks with significant or predominant participation of eclogites; *12* – geological boundaries: (*a*) reverse–thrust and over- and underthrust faults, (*b*) diffuse crust-mantle boundary; *13* – normal-strike-slip (*a*) and inferred transform strike-slip (*b*) faults.

Рис. 11. Разрезы коры и верхней части мантии по профилю FIRE-3-3A: (*A*) геологический, полученный в результате геологической интерпретации сейсмического образа коры; (*B*) плотностной – сечение трехмерной модели коры; показаны главные тектонические границы и некоторые изолинии плотности (в том числе сейсмоплотностной Мохо – 3.24 г/см^3).

1–5 – палеопротерозой: *1–3* – Свекофеннский аккреционный ороген: *1* – гранитоиды Центрально-Финляндского плутона, *2–3* – аккреционный комплекс: пояс Саимаа (*2*), тектонические пластины, перекрытые гранитоидами Центрально-Финляндского плутона, погружающиеся под окраину Карельского кратона (*3*), *4* – осадочно-вулканогенный комплекс пассивной окраины, *5* – гранулит-базитовый комплекс пород нижней коры; *6–7* – архей, гранитогнейсовые комплексы: Кухмо-Сегозерский (*6*), Рануа-Иисалми (*7*); *8–9* – плутоны, предположительно гранитоиды: в аккреционном комплексе (*8*), в верхней части коры (*9*); *10* – акустически прозрачная область в средней-нижней коре, предположительно гомогенизированная в результате высокотемпературного метаморфизма; *11* – мантия (предположительно со значительным или преобладающим участием эклогитов); *12* – главные геологические границы: разломы, преимущественно взбросо-надвигового и надвиго-поддвигового типа (*a*), диффузная граница между корой и мантией (*b*); *13* – разломы: сбросо-сдвиги (*a*), предполагаемые трансформные сдвиги (*b*).

Geodynamics & Tectonophysics 2015 Volume 6 Issue 2 Pages 133–170

10–12 km in FIRE-1 and FIRE-3-3A sections. This conclusion agrees with interpretations in [*Kontinen, Paavola, 2006; Korja et al., 2006*]. The massif overlies the accretionary complex proper represented by the sequence of 10–20 km thick tectonic sheets that consecutively plunge northeastward at angles of 10–12° and make up the crustal section down to the crust–mantle boundary at a depth of more than 60 km. The accretionary complex is traced beneath the margin of the Karelian Craton for more than 150 km.

The subsidence of the tectonic sheets beneath the margin of the Karelian Craton is the main structural feature of the boundary between the Palaeoproterozoic orogen and the Archaean Kola–Karelia continent. It is noteworthy that plunging of the large tectonic sheets is accompanied by thrusting of small fragments of the Svecofennian Orogen over the active margin of the Archaean continent. In particular, the Savo Belt, judging by its position in the section, is the sedimentary fill of the back-arc basin squeezed out on the northeastern and southwestern walls of this basin. The sections along FIRE-1 and FIRE-3-3A seismic profiles show clearly that the margin of the Karelian Craton is broken, and the craton's fragments, including the Ranua and Iisalmi microcontinents and the Palaeoproterozoic Kainuu Belt, are displaced in the northeastern direction and form a crocodile-shaped structure. A similar structure of the boundary between the Svecofennian Orogen and the Karelian Craton was established in the section along BABEL profile [*BABEL Working Group, 1990, 1993; Abramovitz et al., 1997; Lahtinen et al., 2009*].

6. Comparison of the density and geological models of the crust

The complex model of the crust and upper lithospheric mantle in the studied region demonstrates a generalized pattern of rock density distribution because the 3D network used for solution of the inverse gravity problem has low spatial resolution. Nevertheless, this model makes it possible to characterize the crucial spatial and structural relationships of the geological objects localized at various depth levels in the Earth's crust.

It is challenging to compare parameters of the density model with results of the geological interpretation of seismic images of the crust along CMP profiles: 4B [*Mints et al., 2009, 2015*], FIRE-1 and FIRE-3-3A [*Kukkonen, Lahtinen, 2006; Mints et al., 2015*].

6.1. Density layering and structural geological characterization of the crust

The rock density values for the upper part of the 3D model of the Earth's crust (Fig. 5), which are obtained by simulation with an allowance for relationships between density and velocity (Fig. 1), are consistent with the laboratory measurement results for corresponding rocks. Even objects of the real geological medium, which are insignificant in size and comparable in dimensions to a cell in the modeling network, find their mediated inference in the anomalies of density in the upper level of the model. The geological structures formed by rocks variable in density, which make up the upper crust along CMP seismic profiles (Figs. 9–11), are reliably identified by density simulation. In general, there are sufficient grounds to state that the 3D model of the regional deep geological structure discussed in this paper also reflects real density heterogeneities at deeper levels of the crust and upper mantle on a scale of the used network of discretization. It should be noted that by virtue of the known resolution of gravimetric problems [*Aleksidze, 1987; Glaznev, 1999*], which substantially depends on spatial positions of field sources, it is unlikely that in the network assigned for solving inverse problem at the lower levels of the section, decreasing the size of cells may lead to any appreciable increase in minuteness of density models or any closer coincidence of simulation results with CMP models.

The heterogeneities of the crust generalized on a scale of simulation show systematic increase in density with depth along with leveling of lateral variations in density, while the main structural features of the medium are maintained (Figs. 5–7). The sections of the 3D density model along 4B (Fig. 9), FIRE-1 (Fig. 10) and FIRE-3-3A CMP profiles also demonstrate density layering in agreement with general trends. The smoothly bending sections of isodensity surfaces are generally near-horizontally oriented.

At first glance, comparison of the density and geological sections demonstrates that coordination is lacking between the density boundaries (and, correspondingly, the velocity boundaries) and the geological and tectonic boundaries separating the rock complexes differing in composition and age. Such relationships between the images of the crust obtained with refraction and reflection seismic methods were established in various geological situations [*Glaznev et al., 1989; Mitrofanov et al., 1998; White et al., 2000; Kuusisto et al., 2006; Cook et al., 2010*]. Therefore, especially important are evidences for partial coordination of the boundaries of density /velocity layering in the crust, on the one hand, and the geological boundaries identified in CMP profiles, on the other hand.

We have revealed a number of specific structural relationships between density anomalies in the crust and geological boundaries in the section along 4B profile (Fig. 9]:

– within intervals of 0–25 km and 50–90 km along the profile in the upper crust, boundaries of areas with

low-density rocks (< 2.70 g/cm^3) approximately follow geological boundaries identified in the seismic image of the crust;

– in the middle crust within the interval of 55–195 km along the strike, the isodensity contour of 2.85 g/cm^3 plunges from a depth of ~15 km down to 20–25 km, wherein acoustically transparent oval domains interpreted as granitoid plutons in [*Mints et al., 2009, 2015*] are localized;

– abrupt vertical displacement of isodensity contours within intervals of 60–65, 100–110, and 170–180 km along the profiles, where reverse–thrust faults are identified.

In the section along FIRE-1 profile (Fig. 10), the general near-horizontal attitude of isodensity contours is combined with similarity between density anomalies and boundaries of geological bodies:

– at intersections of over- and underthrust dislocations in the crust [*Mints et al., 2009, 2015*] at various depths, the insignificant in amplitude but rather sharp vertical shifts of isodensity contours mimic in a smoothed form the main structural lines in the crust within intervals of 25–35, 45–75, 115–125, 165–175, 215–225, and 320–330 km along the profile.

Similar relationships between the boundaries of density layering, emphasized by the isodensity contours, and the geological boundaries are noted in the section along FIRE-3-3A profile (Fig. 11). Noteworthy is local sinking of the isodensity contour of 2.85 g/cm^3 within intervals of 0–50 km and 130–180 km along FIRE-3 profile due to accommodation of relatively low-density rocks close to the surface.

6.2. Velocity–density Moho discontinuity and crust–mantle boundary

As follows from comparison of density and geological sections along 4B, FIRE-1, and FIRE-3-3A profiles, the morphology of the density image of the crust–mantle boundary depends, to a certain degree, on geological structure of the crust in the boundary zone and the crust–mantle boundary proper.

In 4B profile (Fig. 9), where the crustal base is clearly traced as the lower crustal layer (reflectivity zone), an abrupt increase in density to mantle values (3.24–3.30 g/cm^3) is noted at the bottom of this level at a depth of 40 km; the crust–mantle boundary and Moho discontinuity are coordinated and have flat outlines. In the interval of 160–270 km along the profile, where the mantle is enriched in reflecting elements immediately close to the crust, isodensity contours of 3.00 and 3.24 g/cm^3 plunge from a depth of 38 km to 40–45 km. The increase in the depth of Moho discontinuity in the western segment of the profile is apparently caused by approaching the Svecofennian Orogen.

In the geological section along FIRE-1 profile (Fig. 10), the diffuse crust–mantle boundary has complex indented outlines controlled by consecutive plunging of tectonic elements pertaining to the accretionary complex into the mantle and disappearance of their seismic image in the mantle. The velocity–density Moho discontinuity related to the isodensity contour of 3.24 g/cm^3 is characterized by a flat shape complicated by a series of stepwise bends. The localization of the most distinctly curved isodensity contour is directly related to subsidence of the sheets pertaining to the accretionary complex into the mantle. In the southwestern segment of FIRE-1 profile within the interval of 215–335 km, where the seismic CMP image of these sheets gives evidence of their penetration below the 60-km depth, the isodensity contours of 3.24 and 3.30 g/cm^3 also reach a depth of about 60 km.

A similar pattern is observed along FIRE-3-3A profile (Fig. 11), and the following relationships are observed:

– Moho discontinuity marked by the isodensity contour of 3.24 g/cm^3 plunges to a depth of about 70 km within the interval of 60 km along FIRE-3A profile to 110 km along FIRE-3 profile, where the plunging tectonic sheets also reach a maximum depth;

– the isodensity contour of 3.24 g/cm^3 ascends by 15–20 km at the intersection of the boundary between the Svecofennian Orogen and the Karelian Craton.

In the sections along 4B and FIRE-1 profiles, the density boundaries are ascending to the east, while the tectonic sheets are plunging in this direction. This is especially evident in FIRE-1 profile. In other words, in the region adjoining the boundary between the Karelian Craton and the Svecofennian Orogen, the tectonic sheets comprising the accretionary complex are traced to a greater depth than at a distance from this boundary. As shown below, «dissolution» of the crustal sheets can be explained by transformation of the rocks composing such sheets under conditions of eclogite facies.

7. Thermodynamic conditions and metamorphism in the zone of the crustal–mantle boundary

The 3D thermal and density models of the regional lithosphere make it possible to conduct spatial analyses of thermodynamic conditions at the crustal–mantle boundary. For this purpose, the 3D models are transformed into 2D curves of temperature and pressure variations corresponding to Moho discontinuity. As mentioned above, the isodensity surface of 3.24 g/cm^3 satisfies this discontinuity. The spatial distribution of lithostatic pressure at the level of this surface is shown in Fig. 12, *a*. The lithostatic pressure is computed from the real density of the medium with account of the real topography of the studied area. The

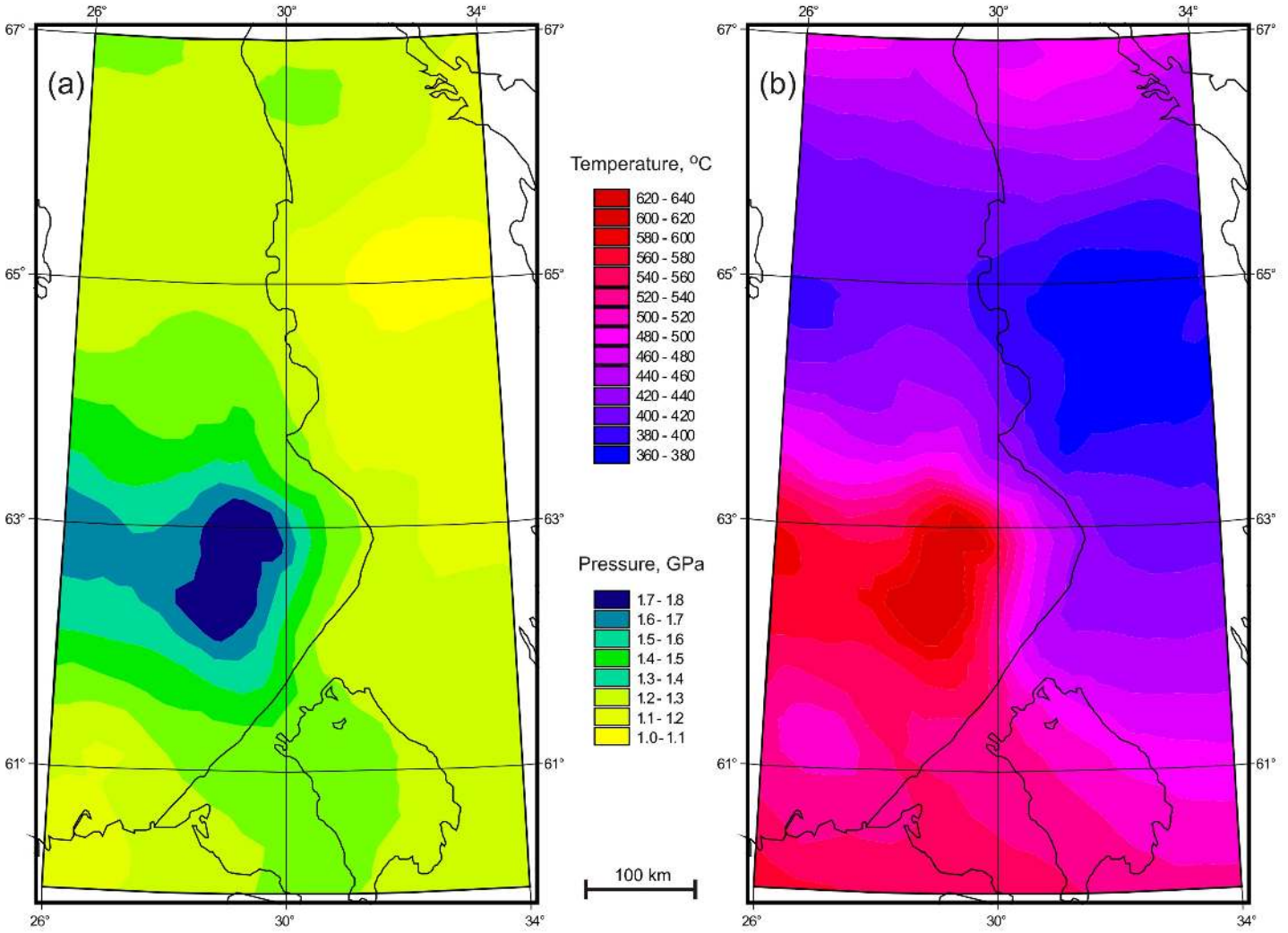

Fig. 12. Distribution of lithostatic pressure (in hPa) (*a*) and temperature (in °C) (b) at the level of the velocity–density Moho discontinuity.

Рис. 12. Термодинамические характеристики сейсмоплотностного раздела Мохо: (*a*) Распределение литостатического давления (в ГПа); (*b*) Распределение температуры (в °С).

estimated lithostatic pressure values range from 1.0 to 1.8 GPa, and this variation is only partly caused by the density anomalies in the middle and lower crust (Figs. 6, 7) and primarily related to significant variations of depth of the velocity–density Moho discontinuity (Fig. 8). In gravity field inversion calculations, pressure determination errors do not exceed ±0.01 GPa.

Spatial distribution of temperature at Moho discontinuity (Fig. 12, *b*) is estimated by interpolation of 3D temperature characteristics of the model at the given depths corresponding to the isodensity surface of 3.24 g/cm^3. Temperatures at this surface range from 360 to 640 °C due to variations of the Moho depth (Fig. 8) and spatial temperature variations in the model (Fig. 4). The temperature determination error is below ±40 °C at the lower levels of the model, which is significantly smaller than the temperature range at the level of the velocity–density Moho discontinuity.

For classification of the obtained estimates of the thermodynamic state of Moho discontinuity, we use the method of group account of arguments [*Ivakhnenko, Yurachkovsky, 1987; Muravina, 2012*] with application of the synergetic approach to establishment of homogeneous groups by model values. According to the pattern of discrete *PT* estimates at the level of the velocity–density Moho discontinuity (Fig. 13, *a*), it is possible to reliably distinguish seven large simply connected spatial domains belonging to six relatively homogeneous physical groups. The same estimates plotted on the *PT* diagram of metamorphic facies are shown in Fig. 13, *b*. The points corresponding to the selected groups are concentrated in the *PT* diagram within two linear belts and two isometric–oval clusters. A regular

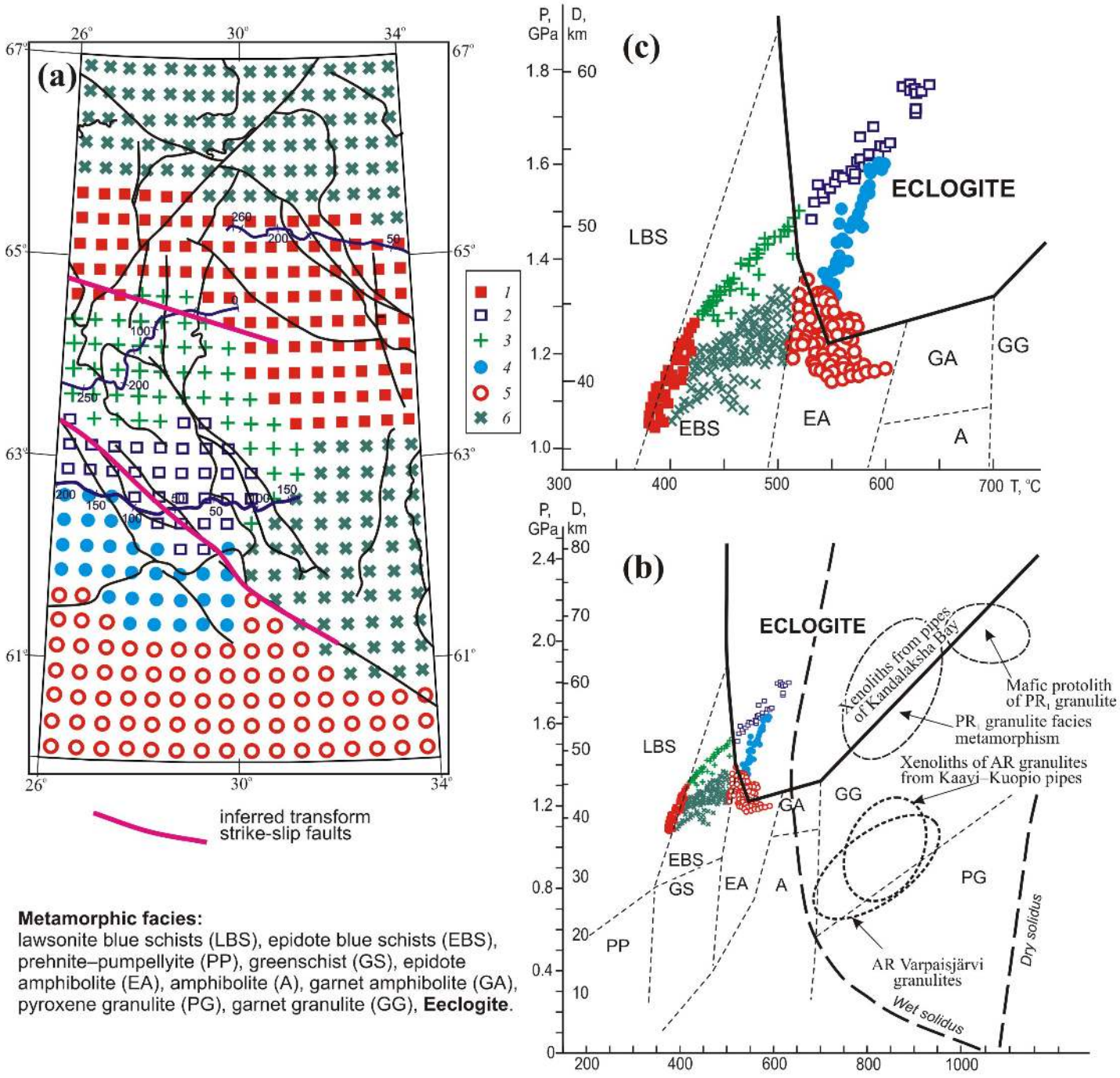

Fig. 13. (*a*) Spatial classification of thermodynamic conditions at the level of the velocity–density Moho discontinuity; (*b*) groups of points for spatial classification of thermodynamic conditions at the level of the velocity–density Moho discontinuity plotted on the *PT* diagram of metamorphic facies, after [*Peacock et al., 1994*]; (*c*) enlarged fragment of the *PT* diagram.

1–6 – groups of points for spatial classification of thermodynamic conditions at the level of the velocity–density Moho discontinuity (explanations are given in the text). Estimates of *PT* parameters for rocks of deep crustal xenoliths: Palaeoproterozoic metagabbroanorthosite and mafic granulites from pipes of Kandalaksha Bay [*Vetrin et al., 2009*]; Archaean granulites from pipes of Kaavi–Kuopio district [*Hölttä et al., 2000b*] and Varpaisjärvi granulites [*Hölttä et al., 2000a*].

Рис. 13. (*a*) Пространственная классификация термодинамических условий на уровне сейсмоплотностного раздела Мохо. (*b*) Положение групп точек пространственной классификации термодинамических условий на уровне сейсмоплотностного раздела Мохо на *PT*-диаграмме метаморфических фаций по [*Peacock et al., 1994*]. (*c*) Увеличенный фрагмент *PT*-диаграммы.

1–6 – группы точек пространственной классификации термодинамических условий на уровне сейсмоплотностного раздела Мохо (пояснения в тексте). Оценки вариаций *PT*-параметров в породах глубинных коровых ксенолитов: палеопротерозойских метагаббро-анортозитов и мафитовых гранулитов из трубок Кандалакшского залива по [*Vetrin et al., 2009*], архейских гранулитов из трубок района Каави-Куопио по [*Hölttä et al., 2000b*]; то же для архейских гранулитов Варпаисъярви по [*Hölttä et al., 2000a*].

distribution of the data points in space and in *PT* coordinates convincingly indicate that the revealed regularities are of real geological significance, as considered below in more details.

(1) Beneath the central part of the Karelian Craton to the north and northeast of the Moho depression, the velocity–density Moho discontinuity is characterized by the group 1 of data points (Fig. 13, *a*) corresponding to the most shallow and colder part of this discontinuity (Fig. 12). In the *PT* diagram, this group is represented by a compact swarm of points, which extends along the boundary between facies of lawsonite and epidote blue schists (Fig. 13, *b*). The swarm is bounded by *T*=370–420 °C and *P*=1.08–1.30 GPa, which correspond to the depth of Moho discontinuity from 36 to 45 km. The minimal depth of Moho discontinuity is established beneath the eastern Karelian Craton (Fig. 13, *a*).

(2) A relatively high-pressure deep linear swarm is represented in the *PT* diagram (Fig. 13, *b*) by groups 2 and 3, which occupy the field corresponding to *T*=410–620 °C and *P*=1.3–1.8 GPa (45–60 km). Groups 2 and 3 characterize the maximal depth of Moho discontinuity (Fig. 12, *a*) related to plunging of the Svecofennian Orogen beneath the western margin of the Karelian Craton (Figs. 7, 10, 11). In the *PT* diagram, this swarm of points is subdivided into two clusters by the boundary of metamorphic eclogite facies at the level of 510–520 °C and 1.55 GPa (~52 km) (Fig. 13, *b*). The high-temperature and high-pressure part of the swarm is located in the field of eclogite facies and represented by group 2 in the diagram; it characterizes the deepest position of the velocity–density Moho discontinuity (52–60 km) (Fig. 12). The second part of the swarm is located in the region of lower temperature and pressure (group 3) and corresponds to facies of epidote blue schists; it characterizes a shallower and less heated part of the velocity–density Moho discontinuity which is located further northward (Fig. 12).

(3) Another high-temperature linear swarm of data points is represented in the *PT* diagram by group 4 (Fig. 13, *b*). It occupies the field corresponding to *T*=530–600 °C and *P*=1.35–1.65 GPa (46–56 km), i.e. the field of eclogite metamorphic facies. The spatial position of the velocity–density Moho discontinuity characterized by this group of data points (Fig. 13, *a*) fits the southern slope of Moho depression (Fig. 8) distinguished by relatively high temperature values (Fig. 12).

To the south and southeast of this region, parameters of the velocity–density Moho discontinuity are characterized by compact group 5 of data points (Fig. 13, *a*). In the *PT* diagrams, this group makes up an isometric oval swarm of points bounded by *T*=500–590 °C and *P*=1.18–1.39 GPa (41–47 km) in the boundary zone between eclogite and epidote-amphibolite facies (Fig. 13, *b*). In geological terms, this field characterizes the Mid-Russia sector of the intracontinental Palaeoproterozoic collision orogen (Fig. 2, *b*) [*Mints, 2007, 2011*].

(4) Group 6 of data points occupies a special position in space. In the *PT* diagram, this swarm is represented by a wide belt of points in temperature and pressure ranges of 380–500 °C and 1.00–1.38 GPa, respectively, which corresponds to the field of epidote blue schists. The Moho discontinuity of this type underlies the northern part of the Karelian Craton and the Belomorian Province, as well as the region to the east of Moho depression (Fig. 13, *a*). The Archaean crust of these tectonic units underwent tectonic and thermal transformation in the Palaeoprotyerozoic [*Bibikova et al., 2001; Mints et al., 2015*].

8. Discussion

The thermal and density models compared with the geological interpretation of the seismic CMP profiles allow us to provide further insight into the structure and physical parameters of the crust and the upper lithospheric mantle of the southeastern Fennoscandian Shield. The seismic sections along the CMP profiles show conventional character of subdivision of the continental crust into the upper, middle, and lower «layers» (Figs. 9–11). Nevertheless, these terms are still in use as being convenient for description of different levels of the crust.

In further discussion, we will focus on consideration of two regions contrasting in their structure and geological history, which are comprehensively presented by the proposed model, specifically the central and eastern parts of the Karelian Craton and the Svecofennian Orogen together with the adjacent margin of the Karelian Craton.

8.1. Density heterogeneity and nature of density layering of the crust

According to the density model, the regional structure of the crust is determined largely by the nearly horizontal boundaries (Figs. 5–7, 9–11), which reflect gradient variations of rock densities with depth. The crustal layers bounded by isodensity surfaces are, as a rule, discordant with respect to the inclined boundaries of geological complexes in seismic images of the crust (Figs. 9–11). As noted above, the density heterogeneities (crustal layers) reveal only local and incomplete interrelations with localization and morphology of the geological bodies.

The isodensity contours in the crustal sections are oriented largely near-horizontally and approximately parallel to the present-day topography, and this is also valid for other Archaean terrestrial cratons [*Abbott et*

al., 2013]. It is evident that only the regional lithostatic pressure remains to be a crucial factor of variations in density of the rocks at the upper and middle crustal levels, where metamorphism is blocked by low temperature (~400 °C in the lower crust and no higher than 300 °C in the middle crust). Density is changing under the lithostatic pressure, while structure of the medium remains intact as formed earlier in the course of sedimentation, magmatic activity, metamorphism, and tectonic reworking. Local factors may include variable crustal and mantle heat flows [*Glaznev, 2003; Glaznev et al., 2004*], zones of stress relaxation [*Lyakhovsky, Ben-Zion, 2009*], and tectonic stresses resulting from interaction of density heterogeneities [*Glaznev et al., 1991; Rebetsky, 2007*]. Rock density increases with increasing depth, while the density differentiation between rocks that differ in compositions is appreciably decreasing [*Glaznev, 2003*].

For long, it has been suggested that the increase in density of the continental crust with increasing depth is determined by variations in composition of the rocks. These ideas were highlighted by the assumption that «granitic» and «basaltic» geophysical layers are separated by Conrad surface in the crust [*Conrad, 1925*]. Despite the fact that conditionality of these terms was always emphasized afterward, the idea of density layering of the continental crust with direct change of its bulk composition has retained its appeal [*Christensen, Mooney, 1995*]. According to [*Kuusisto et al., 2006*], the available information on the crust in the predominant part of the Fennoscandian Shield (including the data discussed in this paper) shows that the layers with different velocities participate in crustal complexes. In the model proposed by M. Kuusisto and co-authors, a contribution of mafic rocks increases with increasing depth; the upper crust consists primarily of gneisses in combination with granite and granodiorite; amphibolite and quartzite are subordinate in abundance; role of amphibolite increases in the middle crust.

We believe, however, that this model cannot represent the structure of the accretionary complex of the Svecofennian Orogen which comprises tectonic sheets plunging beneath the margin of the Karelian Craton and underlying the Archaean rocks of the craton over a significant distance (Fig. 9–11) hardly can be represented. On the contrary, it can be stated that quantitative ratios of different rocks in the plunging tectonic sheets do not undergo any systematic variations either in each particular sheet or in the accretionary ensemble as a whole.

The nature of rock compaction under lithostatic pressure, which is the most important factor determining the state of the continental crust, has been studied insufficiently so far. Since compaction of ancient rocks is controlled by the recent or close-to-recent state of the crust at least for the upper and middle crust, metamorphism (often mentioned as a factor of compaction) should be excluded from the list of potential causes. Undoubtedly important factors are closure of fractures and pores and release of solutions and fluids contained therein. However, all by themselves, such factors are not able to provide for the observed compaction of rocks which is significantly exceeding the results of laboratory experiments on rock samples under elevated pressure (for example, from 2.80–2.85 to 3.0–3.1 g/cm^3 in the case of sedimentary and volcanic rocks of the Svecofennian accretionary complex). It is also noteworthy that the discussed variation in density of rocks is apparently reversible, because the boundaries of the crustal layers with different densities, except for the uppermost ones, are not cut by the erosion topography features, and the density layering pattern is similar for young orogens, undergoing the stage of growth and intense denudation, and for equilibrated isostatic platform regions. Further studies are needed to clarify of the nature of global compaction of the crust.

8.2. Nature of the lower crust, the crust–mantle boundary and the velocity–density Moho discontinuity beneath the Karelian Craton

In seismic CMP sections, the lower crust is commonly identified with a reflectivity zone localized immediately above the crust–mantle boundary, in other words, with a zone of intense seismic reflections that occupy either the entire zone or its major part and depict an image of the layered lower crust [*Mooney, Meissner, 1992*]. Such a reflectivity zone (7–12 km thick) continuously underlies the Archaean crust in the eastern Fennoscandian Shield, including the Karelian and Kola Cratons and the Belomorian Province [*Mints et al., 2009; Mints, 2011*].

In the region considered in this paper, the lower crust of this type is observed in the section along 4B profile (Fig. 9). The pattern of seismic reflections in this section demonstrates an almost horizontal smooth crust–mantle boundary lying at a depth of 37–39 km. In the major segment of 4B profile, the crust–mantle boundary practically coincides with the velocity–density Moho discontinuity (represented by the isodensity contour (surface) of 3.24 g/cm^3) of the similar morphology. In the central part of the Karelian Craton, the Moho depth varies from 38 to 45 km (Fig. 12, *a*). Depths of 42–45 km, which are more significant than those in 4B profile, are characteristic of the Kianta and Iisalmi terranes in the western part of the craton. It should be noted that the depth of Moho in this region is 46–52 km according to the models described in [*Tesauro et al., 2008*] and [*Grad et al., 2009*] or 48–52 km according to [*Kozlovskaya et al., 2004*]. Even a

greater depth of Moho discontinuity is suggested in [*Silvennoinen et al., 2014*]. At the Moho discontinuity of this type, temperature varies in a narrow range from 370 to 420 °C (Fig. 13, *b*, group 1), and such a variation is the lowest as compared to values for other Moho segments. These parameters are consistent with minimal values of heat flow (8÷10 mW/m^2) which are typical of the studied region.

In the eastern Fennoscandian Shield, the lower crust (5–15 km thick) is bounded by the crust–mantle boundary of this type [*Mints et al., 2009; Mints, 2011*]. The increase in thickness of the lower crustal layer is related to hummocking (over- and underthrusting) of tectonic sheets at the crust bottom. In particular, a significant increase of the lower crust thickness (up to 20 km) is noted at the western and southwestern margins of the Karelian Craton along its boundary with the Svecofennian Orogen (Figs. 9, 10). In this region, the lower crustal layer is not only characterized by larger thickness values but is also uplifted due to the mutual over- and underthrusting of the rock complexes pertaining to the Karelian Craton and the Svecofennian Orogen. Two important features should be emphasized. First, the lower crustal layer is cut off by the Palaeoproterozoic volcanic–plutonic associations belonging to the Late Palaeoproterozoic Kainuu Belt. Second, this layer is underlain by tectonic sheets of the Svecofennian accretionary complex. The above implies that the lower crustal layer of the Karelian Craton was formed before the Late Palaeoproterozoic collisional events. Thus, the geological data and the seismic images show that formation of the lower crustal complex was related to under- and intraplating by mantle-derived mafic magmas in connection with development of the Palaeoproterozoic large igneous province in the eastern part of Fennoscandian Shield and the adjacent basement of the Russian Platform [*Mints, 2011*].

The lower crust and underlying upper mantle at the boundary between the Kola Craton and the Belomorian Province are cut through by the Devonian kimberlite and lamproite pipes and dikes outcropped at the coast and on islands of the Kandalaksha Bay (Fig. 2). Among lower crustal xenoliths, garnet granulite is dominant; it is identical to mafic granulites and metagabbro-anorthosites of the Lapland and Kolvitsa–Umba granulite-gneiss belts. Peak parameters of granulite-facies metamorphism of rocks from xenoliths are estimated at 800–950 °C and 14–18 kbar and correspond to depths from 50 to 70 km (Fig. 13, *b*) [*Mints et al., 2007*]. In the present-day structure, these rocks belong to the lower crust and occur at a depth of ~ 45 km [*Mints et al., 2009*]. Zircons from garnet granulite range in age from 2.84 to 0.26 Ga and are concentrated within four discrete time intervals as follows: Neoarchaean (2.84–2.74 Ga), Palaeoproterozoic (2.47–2.41) and (1.83–1.75 Ga), and Palaeozoic (0.33–0.26) [*Vetrin, 2006; Vetrin et al., 2009; Downes et al., 2002, and references therein*]. These dates correspond to the main events in the long history of formation and transformation of the crust. The ages of Early Palaeoproterozoic zircons coincide with ages of the known manifestations of magmatism and high-temperature metamorphism of granulite and eclogite facies [*Mints et al., 2007*], which gave start for the Palaeoproterozoic evolution initiated by mantle plumes responsible for formation of the lower crustal «granulite–mafic» layer. A model of the «layered lower crust», that is formed under extension accompanied by sheetlike intrusions of mafic mantle-derived magma, is described in [*Hollinger, Levander, 1994*]. Similar conclusions concerning the origin of the lower crustal reflectivity zone are stated in [*McBride et al., 2004; Meissner et al., 2006*].

Thus, we have sufficient grounds to infer that the lower crust, unlerlying the Archaean Karelian Craton and represented by a reflectivity zone bounded by the smooth nearly horizontal crust–mantle boundary combined with the velocity–density Moho discontinuity of the first type, was formed in the Palaeoproterozoic as a result of tectonothermal and magmatic processes of plume type.

Correspondingly, the Archaean lithospheric mantle of the Karelian Craton was intensely transformed under the impact of the Palaeoproterozoic plumes. Minimal temperature values at the present-day Moho discontinuity indicate that the heat flow generated by this mantle is minimal too, which is believed typical of the domains of the Archaean consolidation [*Nyblade, Pollack, 1993*].

The crust of the western Karelian Craton in the Iisalmi terrane immediately bordering on the Svecofennian Orogen is also characterized by deep xenoliths carried up by the Late Neoproterozoic kimberlite pipes in the Kaavi–Kuopio area (Fig. 2). The kimberlite pipes are located between FIRE-1 and FIRE-3-3A seismic profiles. As can be seen from the section along FIRE-1 seismic profile, a reflectivity zone is absent at the base of the Iisalmi terrane (Fig. 10). The sole of the Archean complex of rocks in this terrain is located at a depth of no more than 20 km. In the Kaavi–Kuopio area, the thickness of the lower crustal layer and depth of its sole are significantly reduced in comparison with those in the section along FIRE-1 profile. The Archaean crust is underlain by a thick (> 40 km) packet of tectonic sheets pertaining to the Svecofennian accretionary complex, which plunge eastward beneath the Karelian Craton. The high-density (up to 3.0–3.24 g/cm^3) rocks at the base of the crust are conjugated with the Palaeoproterozoic rocks of this complex. Any reader can make the same conclusion by analyzing the geological map (Fig. 2) with respect to the geological sections along FIRE-1 and FIRE-3-3A seismic profiles (Figs. 10, 11).

Deep xenoliths are mainly composed of the Archaean and Palaeoproterozoic mafic granulites; the age of their protoliths reaches 3.7–3.5 Ga [*Peltonen et al., 2006*]. Summing up geochronological data on granulites from xenoliths and the Varpaisjärvi Complex exposed nearby [*Hölttä et al., 2000a*] shows that the age of Archaean granulite-facies metamorphism ranges from 2.7 to 2.6 Ga. The peak parameters of granulite-facies metamorphism estimated from the data on xenoliths are 800–930 °C and 8.4–12.5 kbar (depths of 30–45 km) [*Hölttä et al*., 2000b]. For the Varpaisjärvi Complex, the peak parameters are 800–900 °C and 9–11 kbar (depths of 32–39 km) [*Hölttä, Paavola, 2006*]. An evidence for superposition of the Palaeoproterozoic granulite-facies metamorphism on the Archaean rocks of the Varpaisjärvi Complex in the time interval of 2.5–1.7 Ga was obtained only for xenoliths and was not supported by rocks from the Varpaisjärvi Complex [*Hölttä et al., 2000a; Peltonen et al., 2006*]. In addition, zircons younger 1.85 Ga, which crystallized under the thermal impact following the Svecofennian orogeny, were found in xenoliths.

It is quite evident that xenoliths of granulites from the Kaavi–Kuopio pipes and the Varpaisjärvi granulites belong to the same rock complex, which is occurring now at a relatively high level in the crust and at a significant distance from the crust–mantle boundary. Most likely, these xenoliths should be regarded as relics of the Neoarchaean lower crust rather than fragments of the recent lower crust as suggested in [*Kuusisto et al., 2006; Peltonen et al., 2006*].

8.3. Nature of the lower crust, the crustal–mantle boundary, and the velocity–density Moho discontinuity beneath the accretionary Svecofennian Orogen

In the part of the Svecofennian Orogen, which is neighboring the Karelian Craton, the reflectivity zone is absent, while on the contrary, the lower crust is acoustically transparent and characterized by vaguely oriented dispersed reflections. In [*Korsman et al., 1999*], based on seismic wave velocities, the lower crustal complex is represented by the layer with P-wave velocities ranging from 7.0 to 7.45 km/s, which is presumably composed of anorthosites, mafic and metapelitic granulites, and pyroxenite in the highest-velocity areas. According to calculations based on the model proposed in [*Kuusisto et al., 2006*], the upper part of the lower crust (25–40 km) consists of tonalitic gneiss, amphibolite, mafic garnet granulite and pyroxenite, whereas the lower part of the lower crust is mainly composed of hornblendite, mafic garnet granulite, pyroxenite and mafic eclogite. The authors find a confirmation of their model in the fact that all the above-mentioned rocks, except for eclogite, are identified among deep xenoliths in the Kaavi–Kuopio kimberlite pipes. In our turn, we have to remind that in the preceding section we have tried to show that it is hardly valid to compare the recent high-velocity lower crust with these xenoliths.

In [*Lahtinen et al., 2009*], based on paleogeodynamic reconstruction of the Svecofennian Orogen's history, it is assumed that the acoustically transparent region in the lower part of the crust, which is separated by a diffuse boundary from the accretionary complex (Fig. 10, 11), is primarily composed of mafic granulites, formerly making up a hypothetical Keitele microcontinent, which fragments remain unidentified at the surface. A smaller part of this region is occupied by the oceanic crust that was also metamorphosed under conditions of granulite facies. The inferred situation is comparable with the section of the Trans-Hudson Orogen in North America, where the Archaean crust of the Sask Craton is overlapped almost entirely by tectonic nappes of island-arc complexes [*Baird et al., 1996; Hammer et al., 2010*]. However, the rocks of the Sask Craton are rarely found at the present-day surface; in the seismic section, such rocks are characterized by a complex reflection pattern inherent to the Archaean granite–greenstone domains down to the crust–mantle boundary coinciding with Moho discontinuity.

In our view, the structure of the crust established by geological mapping and recorded in the seismic images is a crucial evidence for reconstruction of the lower crust in the Svecofennian Orogen. The ensemble of the inclined tectonic sheets playing the determinant role in structure of the Svecofennian Orogen is limited from below by the uneven boundary that is serrate in many cases. When approaching the mantle, the image of the sheets becomes diffuse and disappears (as if the sheets are dissolved in the mantle), and the serrate shape of the boundary is generally diffusive. In agreement with the above observations, the calculations of the lower crust and upper mantle densities do not show any significant jump of density at the crust–mantle transition. The same was emphasized in [*Kuusisto et al., 2006*].

The Moho discontinuity at the base of Svecofennian Orogen is classified into two subtypes that are distinctly separated in both the *PT* plot and the geological space. The minimal depth of Moho is estimated at 45 km for both subtypes, wherein the difference in temperature is 90 °C. Obviously, the two subtypes are represented by two independent packets of tectonic sheets that plunge (subduct) eastward beneath the Archaean crust of the Karelian Craton (Fig. 13, *a*). It is also evident that the mantle domains directly underlying these ensembles are characterized by different heat flow values. At a depth of 45 km, the temperature of 410 °C is typical of the colder subtype, whereas 500 °C is typical of the warmer subtype. At a maximal depth

(~60 km), the temperature is estimated at 600–630 °C for both subtypes. The Moho of the hot packet entirely falls in the *PT* field of eclogitic facies, whereas beneath the colder subtype, the Moho is split approximately in twain by the boundary of *PT* field of eclogitic facies: the deeper and more heated part of the Moho surface is characterized by temperature and pressure of eclogite facies, while the other half is under conditions of epidote blue schists (Fig. 13, *b*).

Considering high densities of rocks in the lower crust and the underlying mantle along with the diffusive boundary between them, there are grounds to suggest that similar high-density eclogites participate in either of them.

The limits of corresponding parts of the Moho surface projected on the surface show boundaries of the plunging packets of tectonic sheets. Judging by the configuration of the boundaries, the packets are separated by a transform fault zone striking in the SE direction (Fig. 13, *a*). The width of the northern colder packet amounts to 250 km. The width of the southern warmer packet exceeds 100 km. The maximal depth of the velocity–density Moho discontinuity is somewhat greater than 60 km.

It is noteworthy that the contours of the plunging tectonic ensembles are advanced far away from the boundary between the Svecofennian Orogen and the Karelian Craton, which is observed at the surface. This fact is fully in accordance with the suggested subduction of island-arc, backarc, and interarc basins of the Svecofennian Orogen beneath the margin of the Karelian Craton. It should be specially noted that in regard to subduction, both methods based on refraction and reflection seismic profiling have given strikingly consistent results.

Generally, one of the most plausible scenarios of the Moho discontinuity formation is represented by the model of the crust–mantle boundary assuming transformation of the lower crustal rocks, largely gabbro and basalt (density of 2.8–3.2 g/cm^3) into eclogite (3.3–3.7 g/cm^3), as reviewed in [*Mjelde et al., 2013*]. The model envisages that the Moho boundary separates differently metamorphosed mafic rocks, and eclogites, being the crustal rocks by their chemical composition, are referred to as the mantle rocks by their elastic properties. As a rule, the gabbro–eclogite model of Moho discontinuity is considered in specific geodynamic settings, including continental domains and rift zones, suture zones, and bottom of high-pressure granulite complexes [*Mareschal et al., 1982; Brown, 2009; Mjelde et al., 2013*].

It has been repeatedly noted that the reflection packets plunging into the mantle (similar to those observed along FIRE-1 and FIRE-3-3A profiles, see Figs. 10 and 11) are intersected by Moho discontinuity. This specific feature of the Moho boundary was noted in studies of the Palaeoproterozoic structural units of the Bothnian Bay along BABEL profile [*BABEL Working Group, 1990*] and the Trans-Hudson Orogen along COCORP profiles [*Baird et al., 1995, 1996*], and interpreted as a result of a supra-regional mantle event that occurred after formation of the collision orogen. A partial removal of the eclogitized keel is commonly explained by its subsequent delamination and subsidence into the mantle.

The thorough study of deep xenoliths in the Late Neoproterozoic kimberlite (500–600 Ma) from the Kaavi–Kuopio pipes, however, did not reveal any fragments of crustal eclogites [*Peltonen et al., 2006*]. This fact can be interpreted equivocally. According to the model described in [*Kukkonen et al., 2008*], eclogites were formed at the base of the Late Palaeoproterozoic Svecofennian accretionary complex during subduction and collision with the Karelian Craton. Later on, the lower crust of accretionary complex was subject to delamination; the majority of fragments of the eclogite layer subsided into the mantle, while others were partly disintegrated and thus 'missed' when xenoliths were trapped by the kimberlitic magma. Alternatively, it can be assumed that the lower crust and upper mantle were devoid of eclogites during the period of kimberlite magmatism.

Based on our results of complex 3D simulation, we can pioneer in characterizing the temperature distribution pattern along the Moho surface at the bottom of the crust in the Svecofennian Orogen, including the region of its plunging beneath the continental margin of Karelian Craton. The results of computation (Figs. 12, 13) indicate that the boundary of thermodynamic conditions corresponding to eclogite facies is approximately coincident with the present-day position of the crust–mantle boundary in the Moho depression. Therefore, it can be concluded that eclogite-facies metamorphism may be related to the recent thermal state of the regional lithosphere. At the same time, it should be kept in mind that in the absence of fluid, these conditions are insufficient for the metamorphic reactions to proceed. With account of the fact that the eclogitic model provides explanations for both the high density of the lower crust composed of the accretionary complex, and the diffuse character of the boundaries between the accretionary complex, the lower crust and the mantle, such a model seems quite plausible, yet remains hypothetical. Moreover, differences in the mantle heat flows in the two separate parts of the accretionary complex give evidence in favor of the eclogitic model of the lower crust of the Svecofennian Orogen.

Thus, the complex geophysical 3D model discussed in this paper allows us to suggest that transformation of the volcanic and sedimentary rocks of the lower part of the accretionary complex into eclogites have taken

place in the recent or relatively recent past. In terms of this interpretation, the upper part of the nonuniformly eclogitized rock sequence is represented by acoustically translucent high-velocity and high-density rocks that are regarded as the lower crust, whereas its denser bottom part of the lower crust with predominant eclogite-facies rocks is pertaining to the mantle.

Taking into account the technique of model calculations, it can be assumed that variations in temperature at the level of the velocity–density Moho discontinuity are directly dependent on variations in heat flow from the underlying mantle. With account of specific features of the geological history of the region, it can be suggested that the mantle underlying the Karelian Craton beyond the boundary zone with the Svecofennian Orogen had originated during growth of the continental «nucleus». It was transformed by subduction 3.0–2.8 Ga ago (which has not been reliably characterized yet), modified by high-temperature mantle plumes about 2.7 Ga ago and minimum twice (2.5–2.3 and 2.2–1.8 Ga) in the Palaeoproterozoic.

The mantle underlying the Svecofennian Orogen and its boundary zone with the Karelian Craton was formed at the end of the Palaeoproterozoic during subduction and accretion of island-arc complexes and rocks of back-arc basins. It is evident that this mantle differs from the mantle of the Karelian Craton. Judging by the higher heat flow, the content of heat-generating radioactive elements in the Svecofennian mantle is higher than that in the mantle underlying the Karelian Craton. It is noteworthy that the specific features of the model provide for identification of local differences in heat generation in various part of the Svecofennian mantle.

9. Conclusion

The paper presents results of complex geophysical 3D modelling of the Earth's crust in the Karelian Craton and adjacent regions in the southeastern Fennoscandian Shield. The model is developed with the use of complex inversion of the geophysical data based on the stochastic description of interrelated physical properties of the medium, including density, P-wave velocity and heat generation. For the studied region, the model provides the most comprehensive characteristics of the crust and the upper part of the lithospheric mantle for the Archaean Karelian Craton and Late Palaeoproterozoic Svecofennian Orogen.

The model analyses provide for transition from the averaged characteristics of the temperature field at the Moho that is variable in depth to the 3D representation of temperature variations therein. This, in turn, allows us to characterize regularities in temperature variations at the Moho, separately reconstruct the nature of the Moho for different tectonic units, estimate variations of the mantle heat flow, and consider geodynamic and tectonic causes of the variations.

Based on results of our studies, we make a number of important conclusions concerning both regional and fundamental problems of deep structure of the Precambrian lithosphere:

(1) The seismic–geological models of the crust and the upper mantle, which are based on the results of geological mapping and interpretation of the seismic reflection patterns, demonstrate associations of geological bodies differing in morphology, such as inclined and horizontal layers and tectonic sheets, as well as nearly isometric bodies. The velocity and density models, that are developed by methods of refraction seismic profiling in combination with gravity measurements, demonstrate near-horizontal layering of the geological medium, which formation is directly related to the recent state of the crust, including distribution of lithostatic loading, heat flow, tectonic stresses etc.

(2) Due to lithostatic loading through geological time, rock density progressively increases with depth. Rock density variability decreases with compaction. A high level of rock compaction cannot be explained by 'simple' concepts of metamorphism and/or rock compaction, which are based on results of laboratory studies of samples and relevant computer models. This implies the existence of additional vigorous mechanisms providing for reversible alteration of rocks.

The detailed pattern of density layering indicates displacements in the crust, which deform isodensity surfaces, including the surface of the velocity–density Moho discontinuity. Stepwise bends of the isodensity surfaces are distinctly related to the previously formed zones of tectonic deformations. These bends apparently arose after termination of lithostatic compaction of rocks. The arrangement of dislocations shows that relaxation of recent stresses in the crust occurs as a result of remobilization of older tectonic zones.

(3) Considering the structural–geological and thermodynamic characteristics of the geological boundary between the crust and the mantle and those of the velocity–density Moho discontinuity at the base of the Archaean Karelian Craton and the Palaeoproterozoic accretionary complex of the Svecofennian Orogen, it is revealed that such characteristics are variable, and their spatial relationships differ significantly.

(3.1) The Archaean crust of the Karelian Craton is underlain by the Palaeoproterozoic lower crustal complex of the mantle-plume origin. This complex consists of the Archaean and Palaeoproterozoic mafic intrusive rocks and gabbroanorthosites metamorphosed in the Palaeoproterozoic under granulite-facies conditions. The reflectivity zone corresponding to this complex is separated from the mantle by the near-horizontal flat boundary that is distinctly expressed in the pattern of

seismic reflections. By its position in the section, the crust–mantle boundary is partly coincident with the velocity–density Moho discontinuity; both boundaries are morphologically similar. The depth of the crust–mantle boundary along 4B seismic profile is 38–39 km and varies elsewhere within a relatively narrow interval (38–45 km). Temperatures at the Moho (370 °C and 410 °C at the depth of 38 km and 45 km, respectively) are the lowest in the studied region.

(3.2) In the pattern of seismic reflections, the Late Palaeoproterozoic accretionary complex of the Svecofennian Orogen is separated from the mantle by a wide translucent domain. According to its density of 3.0–3.24 g/cm^3, this domain is regarded as the lower crust, which is separated from the ensemble of inclined tectonic sheets and, from below, from the mantle by the diffuse transitional zone with serrate outlines. The velocity–density Moho discontinuity is generally following the morphology of the crust–mantle boundary in a smoothed form.

(3.3) The well-known «Moho depression» corresponds to the area of subsidence of the Svecofennian accretionary complex in the boundary zone with the Karelian Craton and further beneath its margin. In this area, the accretionary complex comprises two packets of tectonic sheets that are plunging to the east and divided by the SE-trending transform strike-slip fault. The width of the northern packet is 250 km; the width of the southern packet exceeds 100 km. The depth of the velocity–density Moho discontinuity varies from 45 to 60 km in the region of plunging of both packets. The contours of plunging tectonic ensembles advance far to the east relative to the boundary between Svecofennian Orogen and Karelian Craton, and this fact is fully compliant with the concept assuming subduction of the island-arc, back-arc, and inter-arc basins of the Svecofennian Orogen beneath the margin of the Karelian Craton. In regard to evidences of Svecofennian subduction, both methods based on refraction and reflection seismic profiling have given strikingly consistent results.

(3.4) The complex geophysical model of the geological medium reveals fine temperature distinctions for the identified packets of tectonic sheets at the level of the velocity–density Moho discontinuity. At a depth of 45 km, temperatures of 410 °C and 500 °C correspond to the colder and warmer packets, respectively. At the maximal depth for both packets, temperatures amount to 600–630 °C. The relationships between temperature and pressure at the Moho and the lack of eclogites among deep xenoliths in the Late Neoproterozoic kimberlite pipes allow us to suggest a recent age of transformation of volcanic–sedimentary rocks into eclogites in the lower part of accretionary complex. The upper part of the sequence of nonuniformly eclogitized rocks can be regarded as the lower crust, whereas its denser bottom part with predominant eclogite-facies rocks is pertaining to the mantle.

Based on the complex geophysical simulation results and geological interpretation of the obtained 3D model of the crust and the upper mantle in the southeastern Fennoscandian Shield, we arrive at conclusions of the supraregional level:

– Near-horizontal density layering of the continental crust is superposed on the older geological structure, and the features of such layering are primarily controlled by the recent and near-recent state of the crust and may be disturbed by the youngest deformations;

– Fine temperature variations at Moho discontinuity are determined by local variations of heat generation in the mantle, which, in turn, are related to local features of its origin and transformation;

– Interpretations of the lower continental crust as a «reflectivity zone» and as a layer of high density are not completely equivalent. The lower crust occurs everywhere as the deepest and densest element of near-horizontal density layering of the continental crust; within its limits, the degree of compaction can cardinally differ from laboratory estimates based on relationships between rock composition, density and velocity. Conversely, the seismic image of the reflectivity zone is related to quite definite geological phenomena, that are more or less constrained in space, i.e. mainly to magmatic under- and intraplating under conditions of extensional rifting and ascent of mantle plumes, which form the lower crust of granulite–basic type;

– Rocks of platform domains can be transformed into eclogites at certain combinations of the crust thickness and temperature regime at the level of Moho discontinuity. In this case, the crust–mantle boundary is determined by quantitative proportions of rocks that underwent eclogitization or remained unchanged with corresponding shifts of density and velocity;

– A high level of rock compaction in the crust under lithostatic loading cannot be explained in terms of «simple» concepts of metamorphism and/or rock compaction, which are based on results of laboratory studies of samples and relevant computer models. This implies the existence of very powerful additional mechanisms providing for reversible alteration of rocks. Special studies are needed to clarify their nature.

10. Acknowledgements

This study was supported by the Russian Foundation for Basic Research (Projects Nos. 11-05-00110, 11-05-00492 and 15-05-01214) and the Division of Earth Sciences, Russian Academy of Sciences (Program No. 6). The authors thank Victor Popov and Olga Baksheeva who translated the manuscript in English.

11. References

Abbott D.H., Mooney W.D., Van Tongeren J.A., 2013. The character of the Moho and lower crust within Archean cratons and the tectonic implications. *Tectonophysics* 609, 690–705. http://dx.doi.org/10.1016/j.tecto.2013.09.014.

Abramovitz T., Thybo H., Berthelsen A., 1997. Proterozoic sutures and terranes in the southeastern Baltic Shield interpreted from BABEL deep seismic data. *Tectonophysics* 270 (3–4), 259–277. http://dx.doi.org/10.1016/S0040-1951(96)00213-2.

Aleksidze M.A., 1987. Approximate Methods of Solution of Direct and Inverse Gravimetric Problems. Nauka, Moscow, 336 p. (in Russian) [*Алексидзе М.А.* Приближенные методы решения прямых и обратных задач гравиметрии. М.: Наука, 1987. 336 с.].

Artemieva I.M., Thybo H., Kaban M.K., 2006. Deep Europe today: geophysical synthesis of the upper mantle structure and lithospheric processes over 3.5 Ga. In: D.G. Gee, R.A. Stephenson (Eds.), European lithosphere dynamics. Geological Society London Memoirs, vol. 32, p. 11–41. http://dx.doi.org/10.1144/GSL.MEM.2006.032.01.02

BABEL Working Group, 1990. Evidence for early Proterozoic plate tectonics from seismic reflection profiles in the Baltic shield. *Nature* 348 (6296), 34–38. http://dx.doi.org/10.1038/348034a0.

BABEL Working Group, 1993. Deep seismic reflection/refraction interpretation of crustal structure along BABEL profiles A and B in the Southern Baltic Sea. *Geophysical Journal International* 112 (3), 325–343. http://dx.doi.org/10.1111/j.1365-246X.1993.tb01173.x.

Baird D.J., Knapp J.H., Steer D.N., Brown L.D., Nelson K.D., 1995. Upper mantle reflectivity beneath the Williston basin, phase-change Moho and the origin of intracratonic basins. *Geology* 23 (5), 431–434. http://dx.doi.org/10.1130/0091-7613(1995)023<0431:UMRBTW>2.3.CO;2.

Baird D.J., Nelson K.D., Knapp J.H., Walters J.J., Brown L.D., 1996. Crustal structure and evolution of the Trans-Hudson orogen: Results from seismic reflection profiling. *Tectonics* 15 (2), 416–426. http://dx.doi.org/10.1029/95TC02425.

Balling N., 1995. Heat flow and thermal structure of the lithosphere across the Baltic Shield and northern Tornquist Zone. *Tectonophysics* 244 (1–3), 13–50. http://dx.doi.org/10.1016/0040-1951(94)00215-U.

Barton P.J., 1986. The relationship between seismic velocity and density in the continental crust – a useful constraint? *Geophysical Journal of the Royal Astronomical Society* 87 (1), 195–208. http://dx.doi.org/10.1111/j.1365-246X.1986.tb04553.x.

Berzin R.G., Yurov Y.G., Pavlenkova N.I., 2002. CDP and DSS data along the Uchta–Kem profile (the Baltic Shield). *Tectonophysics* 355 (1–4), 187–200. http://dx.doi.org/10.1016/S0040-1951(02)00141-5.

Bibikova E., Skiöld T., Bogdanova S., Gorbatschev R., Slabunov A., 2001. Titanite-rutile thermochronometry across the boundary between the Archaean Craton in Karelia and the Belomorian Mobile Belt, eastern Baltic Shield. *Precambrian Research* 105 (2–4), 315–330. http://dx.doi.org/10.1016/S0301-9268(00)00117-0.

Birch F., 1961. The velocity of compressional waves in rocks to 10 kilobars: 2. *Journal of Geophysical Research* 66 (7), 2199–2224. http://dx.doi.org/10.1029/JZ066i007p02199.

Braile L.W., Chiang C.S., 1986. The Continental MohorovičIć Discontinuity: Results from Near-Vertical and Wide-Angle Seismic Reflection Studies. In: M. Barazangi, L. Brown (Eds.), Reflection seismology: a global perspective. AGU Geodynamics Series, vol. 13, p. 257–272.

Brown M., 2009. Metamorphic patterns in orogenic systems and the geological record. In: P.A. Cawood, A. Kröner (Eds.), Earth accretionary systems in space and time. Geological Society London Special Publications, vol. 318, p. 37–74. http://dx.doi.org/doi:10.1144/SP318.2.

Buyanov A.F., Glaznev V.N., Mitrofanov F.P., Raevsky A.B., 1995. Three-dimensional modelling of the Lapland Granulite Belt and adjacent structures of the Baltic Shield from geophysical data. In: D. Roberts, N. Nordgulen (Eds.), Geology of the eastern Finnmark – western Kola peninsula region. Geological Survey of Norway, Special Publication, vol. 7, p. 167–178.

Buyanov A.F., Glaznev V.N., Raevsky A.B., Skopenko G.B., 1989. Integrated interpretation of gravity, seismic and geothermal data. *Geofizicheskiy Zhurnal* (*Geophysical Journal*) 11 (2), 30–39 (in Russian) [*Буянов А.Ф., Глазнев В.Н., Раевский А.Б., Скопенко Г.Б.* Комплексная интерпретация данных гравиметрии, сейсмометрии и геотермии // *Геофизический журнал*. 1989. Т. 11. № 2. С. 30–39].

Carbonell R., Levander A., Kind R., 2013. The Mohorovičić discontinuity beneath the continental crust: An overview of seismic constraints. *Tectonophysics* 609, 353–376. http://dx.doi.org/10.1016/j.tecto.2013.08.037.

Christensen N.I., Mooney W.D., 1995. Seismic velocity structure and composition of the continental crust: A global view. *Journal of Geophysical Research* 100 (B6), 9761–9788. http://dx.doi.org/10.1029/95JB00259.

Conrad V., 1925. Laufzeitkurven des Tauernbebens vom 28. November, 1923. Mitteilungen der Erdbeben-Kommission der Akademie der Wissenschaften in Wien, Neue Folge, 59 p.

Cook F.A., White D.J., Jones A.G., Eaton D.W.S., Hall J., Clowes R.M., 2010. How the crust meets the mantle: Lithoprobe perspectives on the Mohorovicic discontinuity and crust–mantle transition. *Canadian Journal of Earth Sciences* 47 (4), 315–351. http://dx.doi.org/10.1139/E09-076.

Dolgal A.S., 2002. Computer Technology of Gravity and Magnetic Surveys Data Processing and Interpretation in Mountainous Areas. Mart Publishing House, Abakan, 187 p. (in Russian) [*Долгаль А.С.* Компьютерные технологии обработки и интерпретации данных гравиметрической и магнитной съемок в горной местности. Абакан: ООО "Фирма Март", 2002. 188 с.].

Downes H., Peltonen P., Mänttäri I., Sharkov E.V., 2002. Proterozoic zircon ages from crustal granulite xenoliths, Kola Peninsula, Russia: evidence for crustal growth and reworking. *Journal of the Geological Society, London* 159 (5), 485–488. http://dx.doi.org/doi:10.1144/0016-764901-162.

Galitchanina L.D., Glaznev V.N., Mitrofanov F.P., Olesen O., Henkel H., 1995. Surface density characteristics of the Baltic Shield and adjacent territories. In: D. Roberts, N. Nordgulen (Eds.), Geology of the Eastern Finnmark–Western Kola Peninsula Region. Geological Survey of Norway, Special Publication, vol. 7, p. 349–354.

Glaznev V.N., 1987. About one approach to construction of a consistent model of the Earth's crust. In: V.I. Starostenko (Ed.), Studies of the lithosphere by geophysical methods. Naukova Dumka, Kiev, p. 228–235 (in Russian) [*Глазнев В.Н.* Об одном подходе к построению согласованной модели земной коры // Изучение литосферы геофизическими методами / Ред. В.И. Старостенко. Киев: Наукова думка, 1987. С. 228–235].

Glaznev V.N., 1999. Evaluation of the limits of applicability of stochastic models of potential fields. *Vestnik VSU, Seriya Geologiya* (*Bulletin of Voronezh State University, Geology Series*) (8), 153–156 (in Russian) [*Глазнев В.Н.* Оценка границ применимости стохастических моделей потенциальных полей // *Вестник Воронежского государственного университета, серия Геология*. 1999. № 8. С. 153–156].

Glaznev V.N., 2003. Complex Geophysical Models of the Fennoscandian Lithosphere. K&M Publishing House, Apatity, 252 p. (in Russian) [*Глазнев В.Н.* Комплексные геофизические модели литосферы Фенноскандии. Апатиты: КаэМ, 2003. 252 с.].

Glaznev V.N., Kukkonen I.T., Raevsky A.B., Ekkinen J., 2004. New data on thermal flow in the central part of the Kola Peninsula. *Doklady Earth Sciences* 396 (4), 512–514.

Glaznev V.N., Raevsky A.B., 1991. About the decision of direct tasks of gravimetry on the spherical Earth for gradient-layered models. In: N.V. Sharov, V.A. Glebovitskiy (Eds.), Problems of integrated interpretation of geological and geophysical data. Nauka, Leningrad, p. 183–188 (in Russian) [*Глазнев В.Н., Раевский А.Б.* О решении прямой задачи гравиметрии на сфере для градиентно-слоистых моделей среды // Проблемы комплексной интерпретации геолого-геофизических данных / Ред. Н.В. Шаров, В.А. Глебовицкий. Л.: Наука, 1991. С. 183–188].

Glaznev V.N., Raevsky A.B., Sharov N.V., 1989. A model of the deep structure of the north-eastern part of the Baltic Shield based on joint interpretation of seismic, gravity, magnetic and heat flow data. *Tectonophysics* 162 (1–2), 151–164. http://dx.doi.org/10.1016/0040-1951(89)90361-2.

Glaznev V.N., Raevsky A.B., Skopenko G.B., 1996. A three-dimensional integrated density and thermal model of the Fennoscandian lithosphere. *Tectonophysics* 258 (1–4), 15–33. http://dx.doi.org/10.1016/0040-1951(95)00147-6.

Glaznev V.N., Skopenko G.B., 1991. Thermal model of lithosphere along the European geotransect 3. In: U.I. Moiseenko, V.V. Gordienko (Eds.), Geothermal models of geological structures. VSEGEI, St. Petersburg, p. 25-31 (in Russian) [*Глазнев В.Н., Скопенко Г.Б.* Термическая модель литосферы вдоль европейского геотрансекта 3 // Геотермические модели геологических структур / Ред. У.И. Моисеенко, В.В. Гордиенко. СПб.: ВСЕГЕИ, 1991. С. 25–31].

Glaznev V., Skopenko G., Smolyaninova E., Lyakhovsky V., 1991. Complex geophysical model of the crust for the Baltic profile. Institute of Seismology University of Helsinki, Report S-25, 107–113.

Glaznev V.N., Zhirova A.M., Raevsky A.B., 2008. New data on the deep structure of the Khibiny and Lovozero massifs, Kola Peninsula. *Doklady Earth Sciences* 422 (1), 1150–1152. http://dx.doi.org/10.1134/S1028334X08070349.

Golizdra G.J., 1988. Complex Interpretation of Geophysical Fields in Studying of Deep Structure of the Earth's Crust. Nedra, Moscow, 212 p. (in Russian) [*Голиздра Г.Я.* Комплексная интерпретация геофизических полей при изучении глубинного строения земной коры. М.: Недра, 1988. 212 с.].

Grad M., Tiira T., ESC Working Group., 2009. The Moho depth map of the European Plate. *Geophysical Journal International* 176 (1), 279–292. http://dx.doi.org/10.1111/j.1365-246X.2008.03919.x.

Hammer P.T.C., Clowes R.M., Cook F.A., Van der Velden A.J., Vasudevan K., 2010. The lithoprobe trans-continental lithospheric cross sections: imaging the internal structure of the North American continent. *Canadian Journal Earth Sciences* 47 (5), 821–857. http://dx.doi.org/10.1139/E10-036.

Holbrook W.S., Purdy G.M., Collins J.A., Sheridan R.E., Musser D.L., Glover L., Talwani M., Ewing J.I., Hawman R., Smithson S.B., 1992. Deep velocity structure of rifted continental crust, U.S. Mid-Atlantic Margin, from wide-angle reflection / refraction data. *Geophysical Research Letters* 19 (16), 1699–1702. http://dx.doi.org/10.1029/92GL01799.

Holliger K., Levander A., 1994. Lower crustal reflectivity modeled by rheological controls on mafic intrusions. *Geology* 22 (4), 367–370. http://dx.doi.org/10.1130/0091-7613(1994)022<0367:LCRMBR>2.3.CO;2.

Hölttä P., Huhma H., Mänttäri, I., Paavola J., 2000a. P-T-t development of Archaean granulites in Varpaisjärvi area, Central Finland. II. Dating of high-grade metamorphism with the U-Pb and Sm-Nd methods. *Lithos* 50 (1–3), 121–136. http://dx.doi.org/10.1016/S0024-4937(99)00055-9.

Hölttä P., Huhma H., Mänttäri I., Peltonen P., Juhanoja J., 2000b. Petrology and geochemistry of mafic granulite xenoliths from the Lahtojoki kimberlite pipe, eastern Finland. *Lithos* 51 (1–2), 109–133. http://dx.doi.org/10.1016/S0024-4937(99)00077-8.

Hölttä P., Paavola J., 2000. P-T-t development of Archaean granulites in Varpaisjärvi area, Central Finland. I. Effects of multiple metamorphism on the reaction history of mafic rocks. *Lithos* 50 (1–3), 97–120. http://dx.doi.org/10.1016/S0024-4937(99)00056-0.

Ivakhnenko A.G., Yurachkovsky J.P., 1987. Modeling of Complex Systems by Experimental Data. Radio i Svyaz Publishing House, Moscow, 120 p. (in Russian) [*Ивахненко А.Г., Юрачковский Ю.П.* Моделирование сложных систем по экспериментальным данным. М.: Радио и связь, 1987. 120 с.].

Kartvelishvili K.M., 1983. Planetary Density Model and the Normal Gravitational Field of the Earth. Nauka, Moscow, 93 p. (in Russian) [*Картвелишвили К.М.* Планетарная плотностная модель и нормальное гравитационное поле Земли. М.: Наука, 1983. 93 с.].

Kempton P.D., Downes H., Neymark L.A., Warto J.A., Zartman R.E., Sharkov E.V., 2001. Garnet granulite xenoliths from the northern Baltic Shield – the underplated lower crust of a Paleoproterozoic large igneous province? *Journal of Petrology* 42 (4), 731–763. http://dx.doi.org/10.1093/petrology/42.4.731.

Kobrunov A.I., 1982. About best value solutions to the inverse problem of gravity. *Izvestiya AN SSSR, Seriya Fizika Zemli* (2), 100–107 (in Russian) [*Кобрунов А.И.* О классах оптимальности решений обратной задачи гравиразведки // *Известия АН СССР, серия Физика Земли*. 1982. № 2. С. 100–107].

Kobrunov A.I., 2008. Mathematical Foundations of the Theory of Interpretation of Geophysical Data. ChentrLitNeftGaz Publishing House, Moscow, 288 p. (in Russian) [*Кобрунов А.И.* Математические основы теории интерпретации геофизических данных. М.: ЦентрЛитНефтеГаз, 2008. 286 с.].

Kontinen A., Paavola J., 2006. A preliminary model of the crustal structure of the eastern Finland Archaean complex between Vartius and Vieremä, based on constraints from surface geology and FIRE 1 seismic survey. In: I.T. Kukkonen, R. Lahtinen (Eds.), Finnish Reflection Experiment FIRE 2001–2005. Geological Survey of Finland Special Paper, vol. 43, p. 223–240.

Korja A., Lahtinen R., Heikkinen P., Kukkonen I.N., and FIRE Working Group, 2006. A geological interpretation of the upper crust along FIRE-1. In: I.T. Kukkonen, R. Lahtinen (Eds.), Finnish Reflection Experiment FIRE 2001–2005. Geological Survey of Finland Special Paper, vol. 43, p. 45–76.

Korsman K., Korja T., Pajunen M., Virransalo P., GGT/SVEKA Working Group, 1999. The GGT/SVEKA transect: structure and evolution of the continental crust in the Palaeoproterozoic Svecofennian orogen in Finland. *International Geology Review* 41 (4), 287–333. http://dx.doi.org/10.1080/00206819909465144.

Kozlovskaya E., Elo S., Hjelt S.-E., Yliniemi J., Pirttijärvi M., SVEKALAPKO Seismic Tomography Working Group, 2004. 3-D density model of the crust of southern and central Finland obtained from joint interpretation of the SVEKALAPKO crustal P-wave velocity models and gravity data. *Geophysical Journal International* 158 (3), 827–848. http://dx.doi.org/10.1111/j.1365-246X.2004.02363.x.

Kukkonen I.T., Gosnold W.D., Šafanda J., 1998. Anomalously low heat flow density in eastern Karelia, Baltic Shield: a possible palaeoclimatic signature. *Tectonophysics* 291 (1–4), 235–249. http://dx.doi.org/10.1016/S0040-1951(98)00043-2.

Kukkonen I.T., Kuusisto M., Lehtonen M., Peltonen P., 2008. Layering of eclogitized lower crust: Control on the crust–mantle boundary in the central Fennoscandian shield. *Tectonophysics* 457 (3–4), 111–127. http://dx.doi.org/10.1016/j.tecto.2008.04.029.

Kukkonen I.T., Lahtinen R. (Eds.), 2006. Finnish Reflection Experiment FIRE 2001–2005. Geological Survey of Finland Special Paper, vol. 43, Helsinki, 247 p.

Kuusisto M., Kukkonen I.T., Heikkinen P., Pesonen L.J., 2006. Lithological interpretation of crustal composition in the Fennoscandian Shield with seismic velocity data. *Tectonophysics* 420 (1–2), 283–299. http://dx.doi.org/10.1016/j.tecto.2006.01.014.

Lahtinen R., Korja A., Nironen M., Heikkinen P., 2009. Palaeoproterozoic accretionary processes in Fennoscandia. In: P.A. Cawood, A. Kröner (Eds.), Earth accretionary systems in space and time. The Geological Society, London, Special Publications, vol. 318, p. 237–256. http://dx.doi.org/10.1144/SP318.8.

Ludwig J.W., Nafe J.E., Drake C.L., 1970. Seismic refraction. In: A.E. Waxwell (Ed.), The Sea, vol. 4. Willey, New York, p. 53–84.

Lyakhovsky V., Ben-Zion Y., 2009. Evolving geometrical and material properties of fault zones in a damage rheology model. *Geochemistry Geophysics Geosystems* 10 (11), Q11011. http://dx.doi.org/10.1029/2009GC002543.

Mareschal J.-C., Gangi A.F., Lamping N.L., 1982. The Moho as a phase change: a test of the hypothesis. *Journal of Geophysical Research* 87 (6), 4723–4730. http://dx.doi.org/10.1029/JB087iB06p04723.

Martushko P.S., Prutkin I.L., 2003. Technology of division of the gravitational field sources in depth. *Geofizicheskiy Zhurnal* (*Geophysical Journal*) 25 (3), 30–34 (in Russian) [*Мартышко П.С., Пруткин И.Л.* Технология разделения источников гравитационного поля по глубине // *Геофизический журнал*. 2003. Т. 25. № 3. С. 30–34.].

McBride J.H., White R.S., Smallwood J.R., England R.W., 2004. Must magmatic intrusion in the lower crust produce reflectivity? *Tectonophysics* 388 (1–4), 271–297. http://dx.doi.org/10.1016/j.tecto.2004.07.055.

Meissner R., Rabbel W., Kern H., 2006. Seismic lamination and anisotropy of the Lower Continental Crust. *Tectonophysics* 416 (1–4), 81–99. http://dx.doi.org/10.1016/j.tecto.2005.11.013.

Mereu, R.F., Baerg, J., Wu, J., 1989. The complexity of the continental lower crust and Moho from PmP data: results from COCRUST experiments. In: R.F. Mereu, S. Mueller, D.M. Fountain (Eds.), Properties and Processes of Earth's Lower Crust. AGU Geophysical Monograph, vol, 51, p. 103–119.

Miksat J., Wen K.-L., Wenzel F., Sokolov V., Chen C.-T., 2010. Numerical modelling of ground motion in the Taipei Basin: basin and source effects. *Geophysical Journal International* 183 (3), 1633–1647. http://dx.doi.org/10.1111/j.1365-246X.2010.04818.x.

Mints M.V., 2007. Paleoproterozoic supercontinent: Origin and evolution of accretionary and collisional orogens exemplified in northern cratons. *Geotectonics* 41 (4), 257–280. http://dx.doi.org/10.1134/S0016852107040012.

Mints M.V., 2011. 3D model of deep structure of the Early Precambrian crust in the East European Craton and paleogeodynamic implications. *Geotectonics* 45 (4), 267–290. http://dx.doi.org/10.1134/S0016852111040054.

Mints M.V., Dokukina K.A., Konilov A.N., Philippova I.B., Zlobin V.L., Babayants P.S., Belousova E.A., Blokh Yu.I., Bogina M.M., Bush W.A., Dokukin P.A., Kaulina T.V., Natapov L.M., Piip V.B., Stupak V.M., Suleimanov A.K., Trusov A.A., Van K.V., Zamozhniaya N.G., 2015. East European Craton: Early Precambrian history and 3D models of deep crustal structure. Geological Society of America Special Paper, vol. 510, 433 p. http://dx.doi.org/10.1130/2015.2510.

Mints M.V., Glaznev V.N., Konilov A.N., Kunina N.M., Nikitichev A.P., Raevskiy A.B., Sedykh J.N., Stupak V.M., Fonarev V.I., 1996. Early Precambrian of the North-East of the Baltic Shield: Paleogeodynamics, Structure and Evolution of the Continental Crust. Naucnhyi Mir, Moscow, 287 p. (in Russian) [*Минц М.В., Глазнев В.Н., Конилов А.Н., Кунина Н.М., Никитичев А.П., Раевский А.Б., Седых Ю.Н., Ступак В.М., Фонарев В.И.* Ранний докембрий северо-востока Балтийского щита: палеогеодинамика, строение и эволюция континентальной коры. М.: Научный мир, 1996. 287 с.].

Mints M.V., Kaulina T.V., Konilov A.N., Krotov A.V., Stupak V.M., 2007. The thermal and geodynamic evolution of the Lapland granulite belt: implications for the thermal structure of the lower crust during granulite-facies metamorphism. *Gondwana Research* 12 (3), 252–267. http://dx.doi.org/10.1016/j.gr.2006.10.007.

Mints M.V., Konilov A.N., 2004. Geodynamic crustal evolution and long-lived supercontinents during the Palaeoproterozoic: Evidence from granulite-gneisses belts, collisional and accretionary orogens. In: P.G. Eriksson, W. Altermann, D.R. Nelson, W.U. Mueller, O. Catuneanu (Eds.), The Precambrian Earth: Tempos and Events. Elsevier, p. 223–239.

Mints M., Suleimanov A., Zamozhniaya N., Stupak V., 2009. A 3-D model of the Early Precambrian crust under the southeastern Fennoscandian Shield: Karelia Craton and Belomorian tectonic province. *Tectonophysics* 472 (1–4), 323–339. http://dx.doi.org/10.1016/j.tecto.2008.12.008.

Mitrofanov F.P., Sharov N.V., Zagorodny V.G., Glaznev V.N., Korja A., 1998. Crustal structure of the Baltic shield along the Pechenga – Kostomuksha – Lovisa geotraverse. *International Geology Review* 40 (11), 990–997. http://dx.doi.org/10.1080/00206819809465250.

Mjelde M., Goncharov A., Müller R.D., 2013. The Moho: Boundary above upper mantle peridotites or lower crustal eclogites? A global review and new interpretations for passive margins. *Tectonophysics* 609, 636–650. http://dx.doi.org/10.1016/j.tecto.2012.03.001.

Mooney W.D., Meissner R., 1992. Multi-genetic origin of crustal reflectivity: a review of seismic reflection profiling of the continental lower crust and Moho. In: D.M. Fountain, R. Arculus, R.W. Kay (Eds.), Continental Lower Crust. Elsevier, Amsterdam, p. 45–79.

Muravina O.M., 2012. The method of the group account of arguments in the analysis of geophysical data. *Geofizika* (*Geophysics*) (6), 16–20 (in Russian) [Муравина О.М. Метод группового учета аргументов при анализе геофизических данных // *Геофизика*. 2012. № 6. С. 16–20].

Nyblade A.A., Pollack H.N., 1993. A global analysis of heat flow from Precambrian terrains: implications for the thermal structure of Archean and Proterozoic lithosphere. *Journal of Geophysical Research* 98 (B7), 12207–12218. http://dx.doi.org/10.1029/93JB00521.

O'Reilly S.Y., Griffin W.L., 2013. Moho vs crust–mantle boundary: Evolution of an idea. *Tectonophysics* 609, 535–546. http://dx.doi.org/10.1016/j.tecto.2012.12.031.

Pasquale V., Verdoya M., Chiozzi P., 1991. Lithospheric thermal structure in the Baltic Shield. *Geophysical Journal International* 106 (3), 611–620. http://dx.doi.org/10.1111/j.1365-246X.1991.tb06333.x.

Peacock S.M., Rushmer T., Thompson A.B., 1994. Partial melting of subducting oceanic crust. *Earth and Planetary Science Letters* 121 (1–2), 227–244. http://dx.doi.org/10.1016/0012-821X(94)90042-6.

Pedersen L.B., 1991. Relations between potential fields and some equivalent sources. *Geophysics* 56 (7), 961–971. http://dx.doi.org/10.1190/1.1443129.

Peltonen P., Kontinen A., Huhma H., 1998. Petrogenesis of the mantle sequence of the Jormua Ophiolite (Finland): Melt migration in the upper mantle during Palaeoproterozoic continental break-up. *Journal of Petrology* 39 (2), 297–329. http://dx.doi.org/10.1093/petroj/39.2.297.

Peltonen P., Mänttäri I., Huhma H., Whitehouse M.J., 2006. Multi-stage origin of the lower crust of the Karelian craton from 3.5 to 1.7 Ga based on isotopic ages of kimberlite-derived mafic granulite xenoliths. *Precambrian Research* 147 (1–2), 107–123. http://dx.doi.org/10.1016/j.precamres.2006.02.008.

Prodehl C., Kennett B., Artemieva I., Thybo H., 2013. 100 years of seismic research on the Moho. *Tectonophysics* 609, 9–44. http://dx.doi.org/10.1016/j.tecto.2013.05.036.

Rebetsky Yu.L., 2007. Tectonic Stresses and Strength of Natural Massive. Akademkniga Publishing House, Moscow, 406 p. (in Russian) [*Ребецкий Ю.Л.* Тектонические напряжения и прочность природных горных массивов. М.: ИКЦ «Академкнига», 2007. 406 с.].

Romanyuk T.V., 1995. Seismo-density modelling of the crust and upper mantle along geotransect Quartz. *Fizika Zemli* (9), 11–23 (in Russian) [*Романюк Т.В.* Сейсмоплотностное моделирование коры и верхней части мантии вдоль геотраверса "Кварц" // *Физика Земли*. 1995. № 9. С. 11–23].

Romanyuk T.V., Mooney W.D., Blakely R.J., 2001. Density model of the Cascadia subduction zone. *Izvestiya, Physics of the Solid Earth* 37 (8), 617–635.

Seipold U., 1998. Temperature dependence of thermal transport properties of crystalline rocks – a general law. *Tectonophysics* 291 (1–4), 161–172. http://dx.doi.org/10.1016/S0040-1951(98)00037-7.

Silvennoinen H., Kozlovskaya E., Kissling E., Kosarev G., POLENET/LAPNET Working Group, 2014. A new Moho boundary map for the northern Fennoscandian Shield based on combined controlled-source seismic and receiver function data. *GeoResJ* 1–2, 19–32. http://dx.doi.org/10.1016/j.grj.2014.03.001.

Sharov N.V., Mitrofanov F.P., Verba M.L., Gillen K. (Eds.), 2005. Lithospheric Structure of the Russian Barents Region. Karelian Research Centre RAS, Petrozavodsk, 318 p. (in Russian) [Строение литосферы российской части Баренц-региона / Ред. Н.В. Шаров, Ф.П. Митрофанов, М.Л. Верба, К. Гиллен. Петрозаводск: КНЦ РАН, 2005. 318 с.].

Sobolev S.V., Babeyko A.Y., 1994. Modelling of mineralogical composition, density and elastic wave velocities in anhydrous magmatic rocks. *Surveys in Geophysics* 15 (5), 515–544. http://dx.doi.org/10.1007/BF00690173.

Strakhov V.N., 1990. On linear inverse problems of gravimetry and magnetometry. *Doklady AN SSSR* 311 (6), 1348–1352 (in Russian) [*Страхов В.Н.* О решении линейных обратных задач гравиметрии и магнитометрии // *Доклады АН СССР*. 1990. Т. 311. № 6. С. 1348–1352].

Strakhov V.N., Romanyuk T.V., 1984. Restoration of the density of the Earth's crust and upper mantle according to the DSS and gravimetry I. *Fizika Zemli* (6), 44–63 (in Russian) [*Страхов В.Н., Романюк Т.В.* Восстановление плотностей земной коры и верхней мантии по данным ГСЗ и гравиметрии I. *Физика Земли*. 1984. № 6. С. 44–63].

Tarantola A., Valette B., 1982. Generalized nonlinear inverse problems solved using the least square criterion. *Review of Geophysics and Space Physics* 20 (2), 219–232. http://dx.doi.org/10.1029/RG020i002p00219.

Tesauro M., Kaban M., Cloetingh S., 2008. EuCRUST-07: A new reference model for the European crust. *Geophysical Research Letters* 35 (5), L05313. http://dx.doi.org/10.1029/2007GL032244.

Thybo H., Artemieva I.M., 2013. Moho and magmatic underplating in continental lithosphere. *Tectonophysics* 609, 605–619. http://dx.doi.org/10.1016/j.tecto.2013.05.032.

Tiberi C., Diament M., Déverchère J., Petit-Mariani C., Mikhailov V., Tikhotsky S., Achauer U., 2003. Deep structure of the Baikal rift zone revealed by join inversion of gravity and seismological data. *Journal of Geophysical Research* 108 (B3), 2133. http://dx.doi.org/10.1029/2002JB001880.

Tikhotsky S., Achauer U., 2008. Inversion of controlled-source seismic tomography and gravity data with the self-adaptive wavelet parametrization of velocities and interfaces. *Geophysical Journal International* 172 (2), 619–630. http://dx.doi.org/10.1111/j.1365-246X.2007.03648.x.

Van der Velden A.J., Cook F.A., 2005. Relict subduction zones in Canada. *Journal of Geophysical Research* 110 (B8), B08403. http://dx.doi.org/10.1029/2004JB003333.

Vernant P., Masson F., Bayer R., Paul A., 2002. Sequential inversion of local earthquake traveltimes and gravity anomaly – the example of the western Alps. *Geophysical Journal International* 150 (1), 79–90. http://dx.doi.org/10.1046/j.1365-246X.2002.01694.x.

Vetrin V.R., 2006. Composition and structure of the lower crust of the Belomorian Mobile Belt, Baltic Shield. *Petrology* 14 (4), 415–438. http://dx.doi.org/10.1134/S0869591106040047.

Vetrin V.R., Lepekhina E.N., Paderin I.P., Rodionov N.V., 2009. Stages of the lower crust formation of the Belomorian mobile belt, Kola Peninsula. *Doklady Earth Sciences* 425 (1), 269–273. http://dx.doi.org/10.1134/S1028334X09020214.

White D.J., Forsyth D.A., Asudeh I., Carr S.D., Wu H., Easton R.M., Mereu R.F., 2000. A seismic-based cross-section of the Grenville Orogen in southern Ontario and western Quebec. *Canadian Journal of Earth Sciences* 37 (2–3), 183–192. http://dx.doi.org/10.1139/e99-074.

Glaznev, Victor N., Doctor of Physics and Mathematics, Head of the Chair of Geophysics
Voronezh State University
1 Universitetskaya pl., Voronezh 394006, Russia
✉ e-mail: glaznev@geol.vsu.ru

Глазнев Виктор Николаевич, докт. физ.-мат. наук, заведующий кафедрой геофизики
Воронежский государственный университет
394006, Воронеж, Университетская площадь, 1, Россия
✉ e-mail: glaznev@geol.vsu.ru

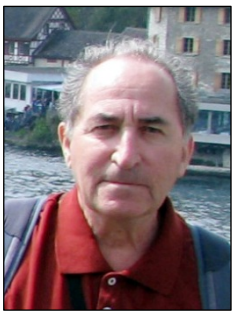

Mints, Mikhail V., Doctor of Geology and Mineralogy, Head of laboratory
Geological Institute of RAS
7 Pyzhevsky lane, Moscow 119017, Russia
e-mail: michael-mints@yandex.ru

Минц Михаил Вениаминович, докт. геол.-мин. наук, зав. лабораторией
Геологический институт РАН
119016, Москва, Пыжевский пер., 7, Россия
e-mail: michael-mints@yandex.ru

Muravina, Olga M., Candidate of Geology and Mineralogy, Associate Professor
Voronezh State University
1 Universitetskaya pl., Voronezh 394006, Russia
e-mail: muravina@geol.vsu.ru

Муравина Ольга Михайловна, канд. геол.-мин. наук, доцент
Воронежский государственный университет
394006, Воронеж, Университетская площадь, 1, Россия
e-mail: muravina@geol.vsu.ru

Raevsky, Aleksei B., Candidate of Physics and Mathematics, Lead Researcher
Geological Institute, Kola Science Center of RAS
14 Fersman street, Apatity 184200, Russia
e-mail: raevsky@geoksc.apatity.ru

Раевский Алексей Борисович, канд. физ.-мат. наук, в.н.с.
Геологический институт КНЦ РАН
184200, Апатиты, ул. Ферсмана, 14, Россия
e-mail: raevsky@geoksc.apatity.ru

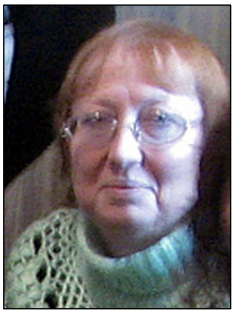

Osipenko, Lyudmila G., Researcher
Geological Institute, Kola Science Center of RAS
14 Fersman street, Apatity 184200, Russia
e-mail: osipenko@geoksc.apatity.ru

Осипенко Людмила Григорьевна, н.с.
Геологический институт КНЦ РАН
184200, Апатиты, ул. Ферсмана, 14, Россия
e-mail: osipenko@geoksc.apatity.ru